EXPERIMENTAL INVESTIGATION: BOUNDARY LAYER FLOW PAST A CIRCULAR CYLINDER MOUNTED ON A FLAT PLATE

A Thesis Submitted
In Partial Fulfilment of the Requirements
for the Degree of
MASTER OF TECHNOLOGY

by

ANIL KUMAR GUPTA

to the

DEPARTMENT OF CIVIL ENGINEERING
INDIAN INSTITUTE OF TECHNOLOGY, KANPUR
JANUARY, 1984

DEDICATED

TO

MY PARENTS

CERTIFICATE

The thesis entitled 'Experimental Investigation: Boundary Layer Flow Past a Circular Cylinder Mounted on a Flat Plate', by Anil Kumar Gupta (Roll No. 8120301) is hereby approved as a creditable report on research carried out and presented in a manner which warrants its acceptance as a prerequisite for the degree of Master of Technology. The work has been carried out under my supervision and has not been submitted elsewhere for a degree.

T. Gangadharaiah 10/1/84

January, 1984

(Dr. T. GANGADHARAIAH)
Assistant Professor
Department of Civil Engineering
Indian Institute of Technology, Kanpur

ACKNOWLEDGEMENTS

The author lacks words to express his sincerest graditude to his thesis supervisor Dr. P. Gangadhariah for his constant help, valuable guidance, inspiration and encouragement during the work.

The author acknowledges his sincere thanks to Dr. V. Lakshminarayana, Dr. K. Subramanya, Dr. S. Surya Rao and Dr. S. Ramaseshan of the Department of Civil Engineering for useful courses he received from them during the degree programme.

The author is thankful to Mr. Suresh Kumar who helped with many of the details of the experimentation. Technical help provided by the staff of the Hydraulics and Water Resources Laboratory of the Department of Civil Engineering and Fluid Mechanics Laboratory of the Department of Mechanical Engineering is greatfully acknowledged.

Special thanks are extended to Mr. B.S. Rohewal for his help provided in Fluid Mechanics Laboratory of department of Mechanical Engineering. The unreserved help received from the friends Mr. R.P. Vyas, Mr. A.K. Yadav, Mr. S.K. Sharma and Mr. R.B.P. Sinha during various stages of work is also acknowledged.

And finally, thanks to Mr. G.S. Trivedi for an excellent job of typing.

Anil Kumar Gupta

CONTENTS

PAGE

LIST OF FIGURES

NOTATIONS

A	Projected area of cylinder
C_D	Local drag coefficient
$\bar{C}_D$	Average drag coefficient
C_p	Coefficient of pressure
$\bar{C}_p$	Average pressure coefficient
C_{po}	Pressure coefficient on the surface of cylinder at $\theta = 0^o$
C_{pmax}	Maximum pressure coefficient (near the corner) on the plate
$\Delta C_{p1}, \Delta C_{p2}, \Delta C_{p3}, \Delta C_{p4}$	Difference in pressure coefficients between crests and troughs of pressure distribution at $\theta = 0$ on the plate
D	Diameter of cylinder
F_r	Froude number $= \frac{U_{ave}}{\sqrt{gh}}$
H	Height of cylinder
R	Radius of cylinder
R_{eD}	Reynolds number $= \frac{U_o D}{\nu}$
$R_{e\delta}$	Reynolds number $= \frac{U_o \delta}{\nu}$
$R^*_{e\delta}$	Reynolds number $= \frac{V_* \delta}{\nu}$
U_o	Free stream velocity
U_{ave}	Average velocity
S	Slope of energy line in uniform channel flows
V_*	Shear velocity
X, Y, Z	Cartesian coordinates with centre of cylinder as orgin

a_o	Distance of separation line on the plate at $\theta = 0^o$ from the centre of cylinder.
a_θ	Radial distance of separation line at angle θ measured from the centre of cylinder
h	Depth of flow of water
h_p	Heads of surface pressure on the model measured with reference to the tunnel pressure
h_v	Dynamic head
r, θ, z	Cylindrical coordinates with the centre of cylinder as origin
$\bar{s}$	Average spacing of streaklines formed on the plate
u, v, w	Velocity components along x,y,z axis respectively
x, y, z	Cartesian coordinates at the station of measurement of velocity profiles
$\frac{\delta}{D} \frac{U_o}{V_*}$	Vorticity parameter
δ	Boundary layer thickness
θ_s	Separation angles on the surface of cylinder
$\bar{\theta}_s$	Average separation angle on the surface of cylinder
ρ	Mass density of fluid
τ_o	Bed shear stress
μ	Dynamic viscosity
ν	Kinematic viscosity
e_s	Blockage correction factor
σ_s	Standard deviation of the spacing of streaklines on the plate

Ω_y — Upstream [illegible] vorticity $= \frac{1}{2}\frac{\partial u}{\partial z}$

Ω_y^* — Non-dimensionalised upstream-[illegible]

Vorticity $= \frac{1}{2}\frac{\delta}{V_*}\frac{\partial u}{\partial z}$

$(\Omega_y^*)_{ave}$ — Average value of non-dimensionalised [illegible] vorticity

Γ — Circulation (strength) of horse-shoe vortices

$\varkappa$ — Kerman constant = 0.4.

ABSTRACT

The investigation presents the analysis of boundary layer flow past the circular cylinder mounted on a flat plate. The flow patterns obtained by paint impression in water flume have been related to the pressure distribution obtained in the wind tunnel. It is observed that the first separation point on the plate upstream of cylinder occurs around $\frac{x}{D} \simeq 1.5$ at $\theta = 0^{\circ}$. The average separation angle on the surface of cylinder varies from 75° to 90° depending upon flow conditions. An increase of average separation angle is observed with the increase of Froude number and Reynolds number of flow. The intense-pressure distribution inside the separation zone on the plate is observed. The presence of three major vortices on the plate at the front of cylinder is postulated from the pressure distributions and flow paint impressions. The strength of horse-shoe vortices has also been related to the pressure distribution on the plate. The vortex centres behind the cylinder are observed near the corner. The average upstream longitudinal vorticity is linearly related to the parameter $\frac{\delta}{D} \frac{V_o}{V_*}$. The drag characteristics of cylinder have also been investigated.

CHAPTER I

INTRODUCTION AND LITERATURE REVIEW

1.1 Introduction:

Cases of three-dimensional flow, where different shaped bodies are connected to one another, and the associated local flow separation, are of common occurrence in engineering practice , for example, the flow around bridge piers. Many investigations have been made on surface pressure distribution, the drag and the wake of a two-dimensional circular cylinder normal to a uniform stream. However, there have been few investigations on flow past a circular cylinder of finite length placed normal to the horizontal plane. From the engineering design point of view, the study of mechanics of flow around such bodies has its own value. For example, scour around bridge piers and abutments is one of the common problems. Separation of flow which generates high strength vortices inside the separating region on the plane surface, is the main cause of local scour around bridge piers. Other engineering examples which are affected by this type of flow are telegraph pole, smoke stack, oil tank and cylindrical building which are all supported on the ground plane.

The investigations on surface pressure distributions and drag for the flow past a circular cylinder mounted on the plate can be related to estimate the air drag of a telegraph pole or a smoke stack because the centre cross-section or the plane of symmetry of the finite circular cylinder may be supposed to be the ground surface. The study of the flow pattern especially inside the separating zone is useful in understanding the mechanism of local scour occuring around bridge piers. From this point of view, the present investigation is carried out to obtain detailed data on the surface pressure distributions, the drag-coefficient and flow pattern inside the separating region for the boundary layer flow past a circular cylinder mounted normal to the flat plate. Belik (1), Okamoto and Yagita (9), and Okamoto (10) are some of the investigators who have carried out experimental study in this field.

Lateral vortex in the incoming boundary layer wraps around the circular cylinder. This vortex is concentrated near the corner of plate and cylinder. The strength of vortex in the separation region must be related to the upstream lateral vortex, and geometry of the cylinder (model). Here an attempt to establish the relation between the lateral vortex and vortex near the corner, has been made. Also an attempt has been made to assess the effect

The investigations on surface pressure distributions and drag for the flow past a circular cylinder mounted on the plate can be related to estimate the air drag of a telegraph pole or a smoke stack because the centre cross-section or the plane of symmetry of the finite circular cylinder may be supposed to be the ground surface. The study of the flow pattern especially inside the separating zone is useful in understanding the mechanism of local scour occuring around bridge piers. From this point of view, the present investigation is carried out to obtain detailed data on the surface pressure distributions, the drag-coefficient and flow pattern inside the separating region for the boundary layer flow past a circular cylinder mounted normal to the flat plate. Belik (1), Okamoto and Yagita (9), and Okamoto (10) are some of the investigators who have carried out experimental study in this field.

Lateral vortex in the incoming boundary layer wraps around the circular cylinder. This vortex is concentrated near the corner of plate and cylinder. The strength of vortex in the separation region must be related to the upstream lateral vortex, and geometry of the cylinder (model). Here an attempt to establish the relation between the lateral vortex and vortex near the corner, has been made. Also an attempt has been made to assess the effect

of boundary layer depth on the vortex characteristics.

1.2 Relevant Literature Review:

The dominant feature of the flow near a pier (cylinder) is the large scale eddy structure or the system of vortices, which develop about the pier. Depending on the type of pier and flow conditions, the eddy structure can be composed of the horse-shoe vortex system and the wake vortex system. These vortex systems are the basic mechanism of local scour, which has long been recognised by investigators like Tison (1940), Keuthner (1932), Posey (1949), Laursen and Toch (1956), Roper and others (1967). The study of horse vortex near the cylinder acting as pier has started recently. [illegible] the investigators who contributed towards this study are Belik, (1973), Okamoto and Yagita (1973) and Okamoto (1978).

Belik, 1973 (1) **Carried out** an experimental study of the vortex systems generated in the region where an incompressible flow with spanwise varying velocity moves about a circular cylinder mounted on a flat plate. He related the horse-shoe vortex generated at the front of the cylinder with the dimensionless similarity numbers describing the flow. Okamoto and Yagita, 1973 (9) carried out an experimental investigation of the flow past a circular cylinder of finite length mounted on the plane surface in a uniform stream. They investigated the effect of H/D ratio

(aspect ratio) on the flow characteristics around the cylinder. Okamoto, 1981 (10) carried out the same type of investigation of the flow behind hemisphere cylinder placed on the ground plane. He compared the results of a hemisphere cylinder with those for a sphere and a circular cylinder of aspect ratio one. A semi-theoretical analysis of open channel flow past circular cylinders was carried out by Rana (15). He interrelated the afflux, the drag forces on the cylinders and the energy loss in such flow problems. Pillai (12) conducted an experimental investigation of free-surface flow past circular cylinders at different blockages. He investigated the drag characteristics of cylinders, the afflux and the energy loss associated with the flow past circular cylinders in open-channels having smooth as well as rough beds.

Different characteristics of flow associated with the flow past a circular cylinder mounted on the plate are reviewed briefly in the following sections.

1.2.1 Pressure Distributions:

(A) On the Surface of Cylinder:

The pressure-distribution for ideal fluid flow, around the two dimensional circular cylinder is given as

$$C_p = \frac{P-P_o}{\frac{1}{2}\rho U_o^2} = (1-4 \sin^2\theta) \qquad (1.1)$$

Thus $C_p = 1$ at $\theta = 0, \pi, 2\pi$

$C_p = -3$ at $\theta = \pi/2, 3\frac{\pi}{2}$

But, for the boundary layer real fluid flow, around the cylinder mounted on a flat plate the pressure distribution is governed by mechanism of three dimensional flow and by the local flow separation. In general, the pressure-recovery at $\theta = 0$ takes place within the boundary layer along the height of cylinder. Some of the investigators have carried out experimental study of pressure distributions on the surface of cylinder for such cases. Okamoto and Yagita (9) also studied the effect of H/D ratio (aspect ratio) on the surface pressure distribution. The surface pressure, the local drag coefficient and the mean drag coefficient change greatly with the aspect ratio between H/D = 6 and 7. Sankaranarayana (12) concluded from his investigation in open channels that the magnitude of maximum C_p, is generally less than the true stagnation pressure and the minimum value of C_p occurs between $\theta = 70^o$ to 90^o.

(B) Pressure Distribution on the Plate:

The pressure distribution in two dimensional potential flow on the plate is given as (1)

$$C_p = \frac{2\text{Cos}(2\theta)}{(r/R)^2} - \frac{1}{(r/R)^4} \qquad (1.2)$$

where C_p is the pressure coefficient, R is the radius of cylinder, r is the radial distance measured from the centre of cylinder at angle θ from the direction of flow.

From the above equation, for $\theta = 0$, at $\frac{r}{R} = 1$ (at corner), $C_p = 1.0$ and the pressure distribution follows a smooth curve. But due to occurrence of separation and vortices on the plate, the distribution does not follow a smooth curve, but fluctuations, in distribution of pressures are generally observed.

1.2.2 Drag Characteristics:

(A) General:

The component of force in the direction of flow exerted by the fluid on the submerged object is called the drag force (F_D). There are two types of drag namely:

(a) Surface or friction drag: In the boundary layer zone, even for the fluids of low viscosity, on account of large velocity gradient, considerable shearing stresses are caused. These shearing stresses exert a tangential force on the object, which is known as surface or friction drag. The development of boundary layer is, therefore, one of the ways in which viscosity of the fluid exerts drag on the objects.

(b) Form or pressure drag: The effect of separation of flow on the obstruction is the cause of form or pressure drag. With the separation of flow, the flow pattern is considerably modified and hence the pressure distribution is changed. On the down-stream side of the body, on account of separation, a region of low pressure is developed which is

known as 'wake'. Since on the upstream side of the body the pressure is considerably high, there exists a pressure difference between the upstream and downstream sides. The pressure difference so created results in a force acting on the body, which is known as form or pressure drag.

Thus, total drag = friction drag + form drag.

The total drag force (F_D) is expressed as

$$F_D = C_D \cdot \frac{A \rho U_o^2}{2} \qquad (1.3)$$

where C_D is drag coefficient, 'A' is the projected area of the body, 'ρ' is the density of fluid and U_o is the free-stream velocity. For the present analysis of drag-characteristics, the form drag has been used since friction drag is very small.

(B) Drag Characteristics of Two Dimensional Cylinder:

The drag coefficient (C_D) of two-dimensional circular cylinder held in the free-stream varies with Reynolds number ($R_{eD} = \frac{U_o D}{\nu}$). The drag coefficient decreases with increase of Reynolds number and reaches a minimum value of about 0.95 at $R_{eD} \simeq 2000$ and then there is a slight rise to 1.2 for $R_{eD} \simeq 3 \times 10^4$. The reason for this rise in the value of C_D is the increasing turbulence in the wake and also the widening of the wake due to the separation points gradually advancing upstream. At $R_{eD} \simeq 2 \times 10^5$, the boundary layer which was upto

now laminar, becomes turbulent before separation and therefore there is a drop in the value of C_D from 1.20 to about 0.3. However, with a further increase in R_{eD} the value of C_D increases gradually from 0.3 to about 0.7 over the approximate range of $5 \times 10^5 < R_{eD} < 3 \times 10^6$. Thereafter since viscous effects are relatively small, it is probable that C_D is practically independent of R_{eD}.

(C) Local Drag Coefficient:

For the cylinder held in the boundary layer flow, the drag coefficient varies along its height. Okamoto and Yagita (9) showed that the local drag coefficient C_D has the maximum value in the neighbourhood of the free end of the cylinder. They also studied the variation of local drag coefficient C_D along the height of cylinder for different H/D (aspect) ratios. Rana (15) found that the local drag coefficient of the cylinders in open channel flow shows little variation with depth for $z/h \geq 0.30$. At lower values of z/h, the local drag coefficient is dependent on the elevation from the bed apart from blockage and flow parameters (h is average depth of uniform flow and z is the distance from the channel bed). Masch and Moore(7) conducted an experimental study of the drag on circular cylinders in velocity gradient flow and found that, a large velocity gradient results in pronounced variation of local drag coefficient over the height.

(D) Average Drag Coefficient ($\bar{C}_D$):

Okamoto and Yagita showed the variation of the average drag coefficient $\bar{C}_D$ with aspect ratio H/D. Rana (15) concluded that the average drag coefficient over the height is dependent on Reynolds number, blockage ratio, Froude number and h/D.

1.2.3 Effect of Blockage:

Since the present investigation is conducted in the wind-tunnel, therefore, a review of effect of blockage on the pressures and drag-coefficients is necessary. Several investigators have studied the effect of blockage on the drag coefficient of circular cylinder. Ramamurthy and Ng(14) have studied experimentally in a wind tunnel the effect of blockage on drag coefficient of smooth circular cylinders placedin uniform flow in subcritical range of Reynolds numbers ($< 10^5$). In particular, the drag, the magnitude of the base pressure and minimum pressure-coefficients increase with increasing blockage. Raju and Singh (16) suggested an empirical relation in the form of a power law as follows:

$$\frac{C_{Do}}{C_D} = \left(1 - \frac{D}{B}\right)^n \qquad (1.4)$$

where C_{Do} is drag coefficient corrected for blockage ratio D/B. C_D is uncorrected drag coefficient. The value of

exponent 'n' depends on body shape. Rana (15) arrived at the following exponential relationship:

$$C_{Do} = C_D \left(1 - \frac{D}{B} \right)^{1.35} \qquad (1.5)$$

1.2.4 Separation Characteristics:

(A) General:

The classical concept of flow separation is due to viscosity; therefore it is often expressed as 'boundary layer flow separation'. In addition, a necessary condition for flow separation is the adverse pressure gradient. The classical concept of flow separation is valid for two-dimensional and axisymmetric flow. In three-dimensional flow, separation can occur with no reverse flow and zero friction, therefore a more generalized and new approach is needed to describe and define three-dimensional flow separation. The approach for the three-dimensional flow separation has been given by many investigators. Eichelrenner and Oudart (2) proposed that the criterian of separation in three dimensional flow should be set-up on the condition that the line of separation must be an envelop of the surface stream lines in the solid surface. The surface-stream lines are defined as flow direction of particles infinitesimally close to the wall. The present investigation is affected by the three dimensional flow separation.

(B) Separation on the Surface of Cylinder:

In a range of Reynolds numbers of 10^3 - 10^5, the flow separation is of laminar nature but the wake is turbulent. The location of laminar separation point in a two-dimensional cylinder is at $\theta = 80^{\circ}$-85°. At large Reynolds numbers (larger than 10^5) the flow in the boundary layer becomes turbulent and the separation point moves down-stream and locates at about 110°. The wake-region reduces greatly in comparison with the laminar separation. The reason for the shifting of separation point further downstream in the turbulent flow is the vigorous-momentum exchange of turbulence taking place. Because of such an exchange, the turbulent flow is more capable of resisting adverse pressure gradient and friction, and flow separates further downstream compared to the laminar flow. Okamoto and Yagita (9) investigated that the separation point of the finite cylinder moves forward with a decreasing H/D (aspect ratio) except in the neighborhood of the free end.

(C) Separation on the Plate:

Due to presence of an obstruction to the flow, pressure on the plate at the front of obstruction is built up. This

building up of pressure, causes the flow to separate on the plate around the obstruction. Sarohia and Young (18) showed in their investigation that the first peak in the pressure distribution on the plate at $\theta = 0$ occured at or little ahead of the first separation line. Belik (1), on the basis of experimental evidence, concluded that for both laminar and turbulent flow the separation region can be characterised by a single similarity number- the vortex fourier number or the Reynolds number based on boundary layer thickness. The limit streamlines forming an 'envelop', i.e. the primary line of separation, upstream of cylinder can well be approximated by a circle within a range of $-60^{\circ} < \theta < 60^{\circ}$, which is not always concentric with the cylinder. In their studies of the laminar boundary layer on a flat wall, Peak and Galway (1) found the primary separation line to be circular for $-80^{\circ} < \theta < 80^{\circ}$. Okamoto(10), in his visualisation experiments in water, showed that the separation line on the plate was located at $\frac{X}{D} \approx 1.6$ upstream of the centre of cylinder.

1.2.5 Vortices:

(A) Vortices on the Plate:

The way that viscous ground plane flows can enter into and establish a vortex core is shown in Figs.1.1(a), 1.1(b) (3). These show the roll-up of boundary layer

Figure 1·1a Side view of the vortex structure ahead of an obstacle

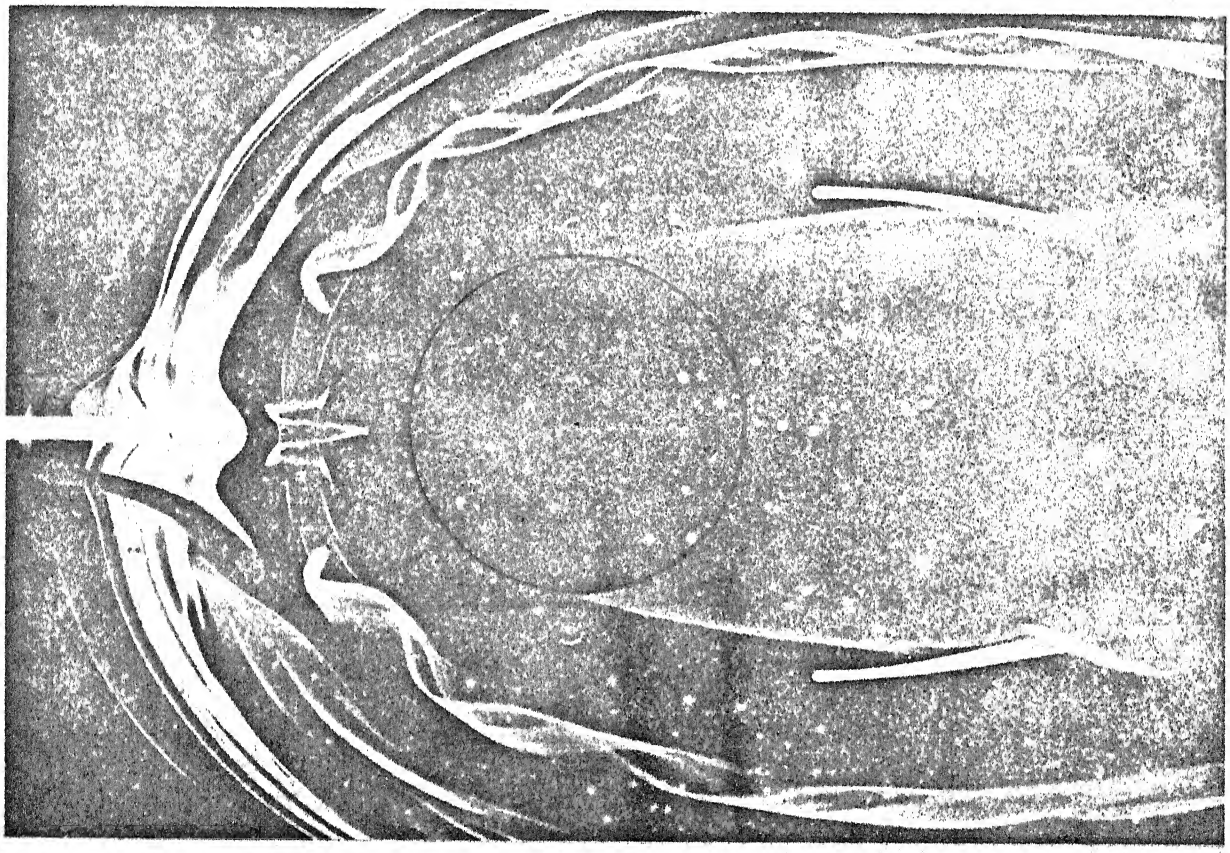

Figure 1·1b The vortex ahead of an obstacle immersed in a boundary layer

ahead of an axisymmetric obstacle that is immersed deep in boundary layer flow. The incoming boundary layer is forced to separate ahead of the obstacle and divide as it passes around the object. This leads to the generation of one or more vortices ahead of the object and wrapped around it. Thus the vortices generated inside the separation region on the plate at the front of obstruction are called 'horse-shoe' vortices. Sarohia and Young (18) found that separated flow involved two main reverse flow vortices, and two small vortices of opposite sign to the main ones, one between the main ones and the other deep in junction. Belik determined the position and size of the vortex core from the measurements of static pressure on the flat wall in the separation region. He showed that the horse-shoe vortex core was shaped like a concentric circle and its position was around $r/R \approx 1.43$ from the centre of cylinder. (R is the radius of cylinder).

(B) Effect of 'Horse-shoe' Vortices:

The core-wise flow in the 'horse-shoe' vortices generated in the separation region on the plate in front of the cylinder is very strong and their structures are remarkably stable. In fact, it is this very characteristic that can have important consequences on obstacles such as bridge piers subject to strong tidal influences. The footing

of the pier becomes steadily eroded by the vortex flow and the pier may eventually become loosened. Thus, these vortices cause the local scour around bridge piers; as a result of it, the stability of piers is affected.

(C) Vortices on the Surface of Cylinder:

Okamoto (10) investigated the existence of 'Arch' vortices, generated behind the separation line on the surface of cylinder. The arch-vortices are shed downstream and are gradually inclined by a strong down-wash behind the cylinder, until they almost touch the ground plate. He also showed that there were two areas in which the pressure was lowest on the ground plate. It is within these two areas that the roots of the arch vortices are attached to the ground plate. It is expected that the 'arch' vortex rotates about these attachment points and is then gradually inclined. Okamoto and Yagita showed that shedding of these vortices from the cylinder occured at a height of around $Z/D \approx 4.0$.

1.3 Present Investigation:

The present investigation consists of the visualisation of flow in the water flume and analysis of boundary layer flow past the circular cylinder mounted on a flat plate. Analysis part has been conducted in the wind tunnel. Analysis of flow

consists of determining pressure distributions on the plate and surface of the cylinder, drag and vortices characteristics. The flow patterns obtained in the water flume have been related to the flow analysis conducted in the wind tunnel. Here an attempt to relate longitudinal vortex in U/S boundary layer flow and the vortex near the junction has also been made. Efforts have also been made to relate the vortices generated in the separation region on the plate to the pressure distribution on the plate.

The boundary layer thickness has been varied from 0.47 D to 2.2 D and its effect on the vortex characteristics has also been investigated. The Reynolds number (R_{eD}) is kept around 0.6×10^5.

CHAPTER II

EXPERIMENTAL METHODS

The experiments for the present investigation are conducted in wind tunnel and water flume. Description of experimental setups, details of the model, measurement of the pressures and velocity profiles, and visualisation techniques are presented in the following section.

2.1 Details of the Wind Tunnel:

The open-circuit wind tunnel with closed test section has been used for the measurement of pressure around the model and upstream flow velocities. Wind tunnel consists of a honeycomb, which is located at one end of the wind tunnel through which air enters into the test section. Just parallel to the honeycomb, there are five screans of size 1.25 m x 1.25 m. After this there is the contraction and then the test section of cross-section 0.4m x 0.4m starts, and the total length of test section is 4.0 m. At the end of the test section, there is gradual expansion from a square test section to a circular section of diameter 1.0 m in a length of 3.0 m. At this end an exhaust fan of 1.0 m diameter is fitted which sucks air through the test section. The exhaust fan is operated by a motor of 3.7 KW, 5 hp and 960 rpm. The motor is connected to a supply of

400 volts through a voltage stabiliser ensuring constant speed.

At the end of the test section, an arrangement with a pair of adjustable gates is provided to control the velocity of air through the test section. The gates can be opened to allow the outside air to enter the tunnel, thus reducing the velocity of air in the test section.

Six different free stream velocities in the range varying from 6.0 m/sec to 20.0 m/sec were used corresponding to the different gate openings. The piezometric tappings are provided on the side of the test section for the static pressure measurements. A slot of 12 mm width is made in the roof of the test section, for the operation of pitot tube in the velocity profile measurements. A layout of the wind tunnel is shown in Fig. 2.1. Figure 2.2 shows the photograph of the experimental setup in the wind tunnel with its accessories.

2.2 Details of the Water Flume:

For the visualisation techniques, in the present investigation, the rectangular water flume of 15 cm width and 3.0 m length has been used. The system of flow straighteners are located at the upstream end of the flume. The water is pumped by a motor through venturimetered pipe

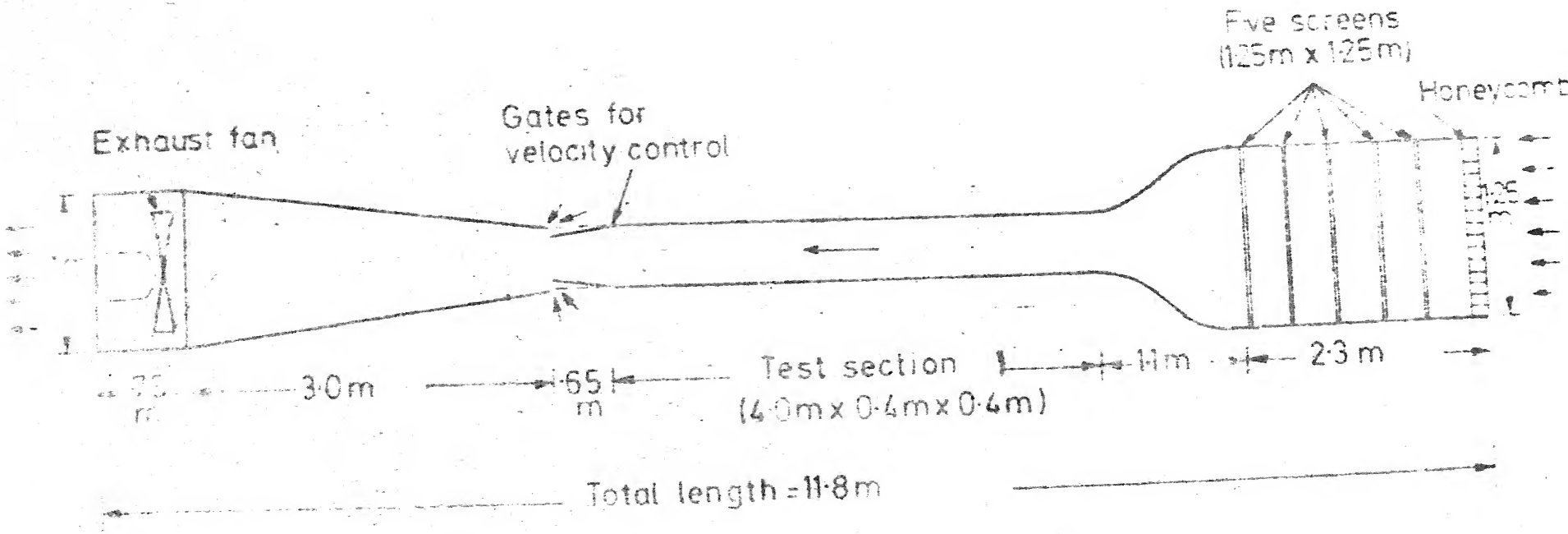

FIG.2 LAYOUT OF WIND TUNNEL

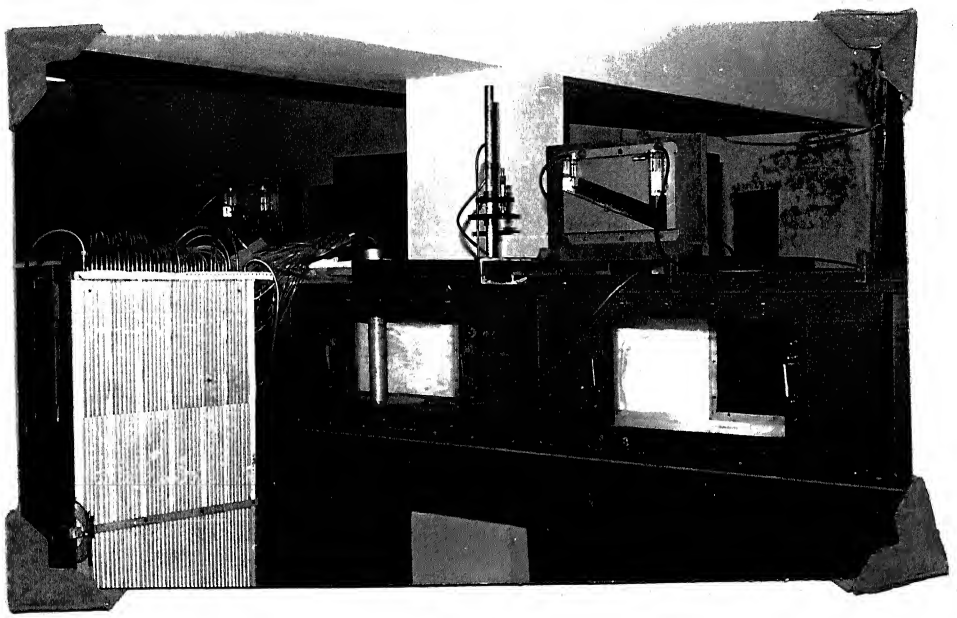

FIG. 2.2 : GENERAL VIEW OF EXPERIMENTAL SET-UP IN WIND TUNNEL

which enters into the test section via flow straightners for maintaining more or less constant depth of flow.

To control the velocity and depth of flow keeping discharge constant, a drilled aluminium plate of 0.15x0.30 m section is used at the downstream end. The discharge is controled by sluice valve fitted in the supply pipe. The flume body is resting on the lever at the centre and is simply supported at the upstream end. The downstream end was cantilevered, which has been made simply supported to remove the defect of bending by self load of flume and the live load of water. The point gauge has been used for measuring the depth of flow which can move along the flume length. The test station for the flow visualisation has been chosen at 2.00 m downstream from the inlet. A layout of the water flume used is shown in Fig. 2.3.

2.3 Details of the Model:

An aluminium pipe of 5.0 cm diameter and 30 cm height (acting as cylinder) mounted on a circular aluminium plate of diameter of about 25 cm has been used for the present investigation in the wind tunnel. This combination is kept on the wooden boards kept at 5 cm above bottom of the wind tunnel acting as a bed. The test plate has 19 tappings from the corner of cylinder to the edge of the plate. These

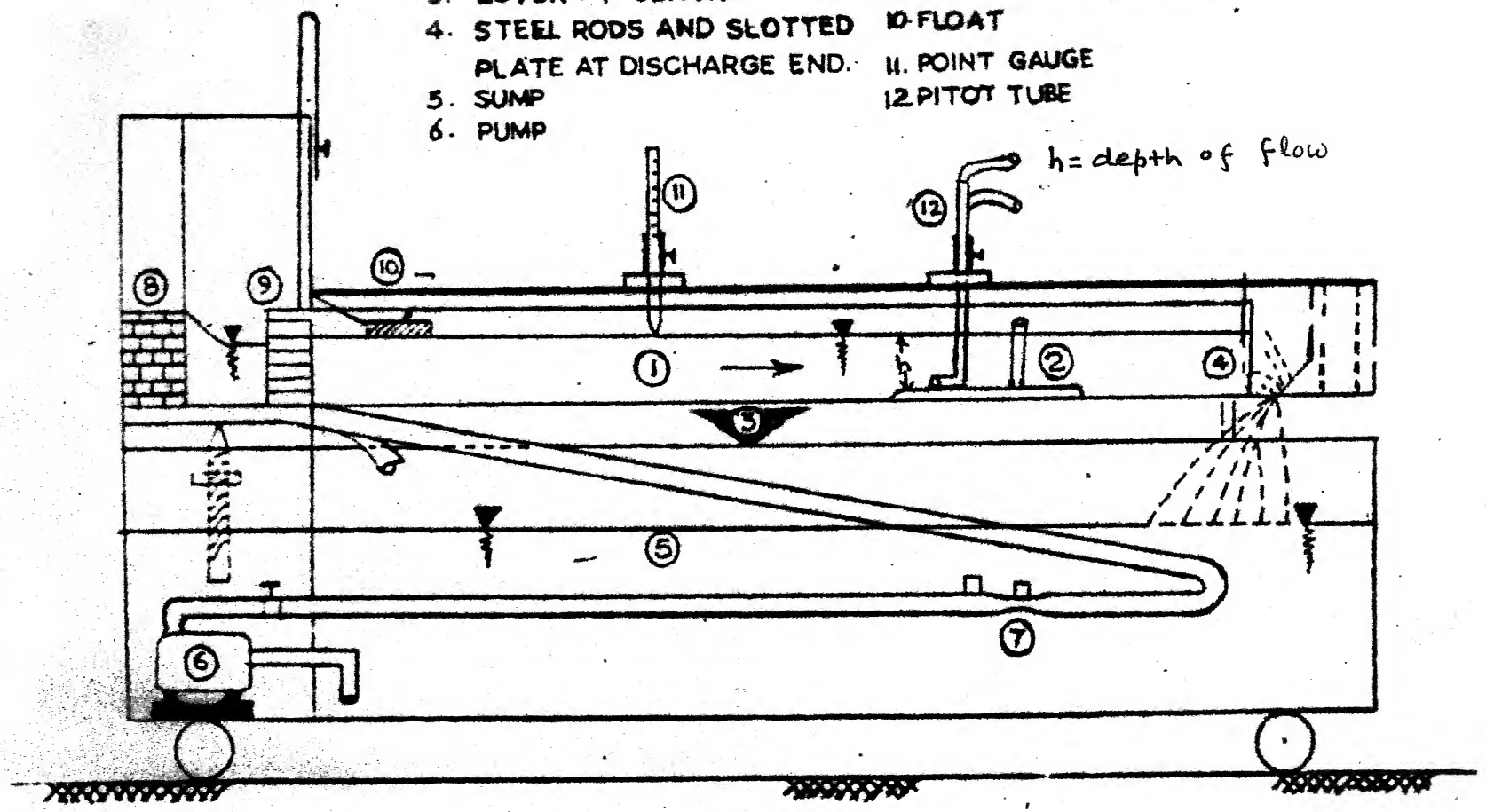

FIG 23 LAY OUT OF EXPERIMENTAL WATER FLUME

holes are equally spaced in one line having spacing of 5 mm c/c (equal to 0.1 D) each. Similarly the cylinder also has 22 holes along its height. The first 10 holes from the bottom are spaced at 5 mm each c/c , next 5 at 10 mm each c/c and last 7 at 20 mm each c/c. These holes are connected to the tubes to measure the pressures. The cylinder along with the bottom plate can be rotated at any angle on the wooden board.

The spacing of pressure holes on the bottom plate and along the height of cylinder used in wind tunnel is summarised below:

Bottom plate	:	Total number of holes	-	19
		Spacing	-	5 mm each c/c(0.1D)
Cylinder	:	Total number of holes	-	22
		Spacing (first 10)	-	5 mm each c/c(0.1D)
		(next 5)	-	10 mm each c/c(0.2D)
		(last 7)	-	20 mm each c/c(0.4D)

Figure 2.4 shows details of the model used in wind tunnel.

The model used in the visualisation technique consists of a pipe acting as a cylinder of 2.5 cm diameter and 14.5 cm height attached to a rectangular aluminium plate

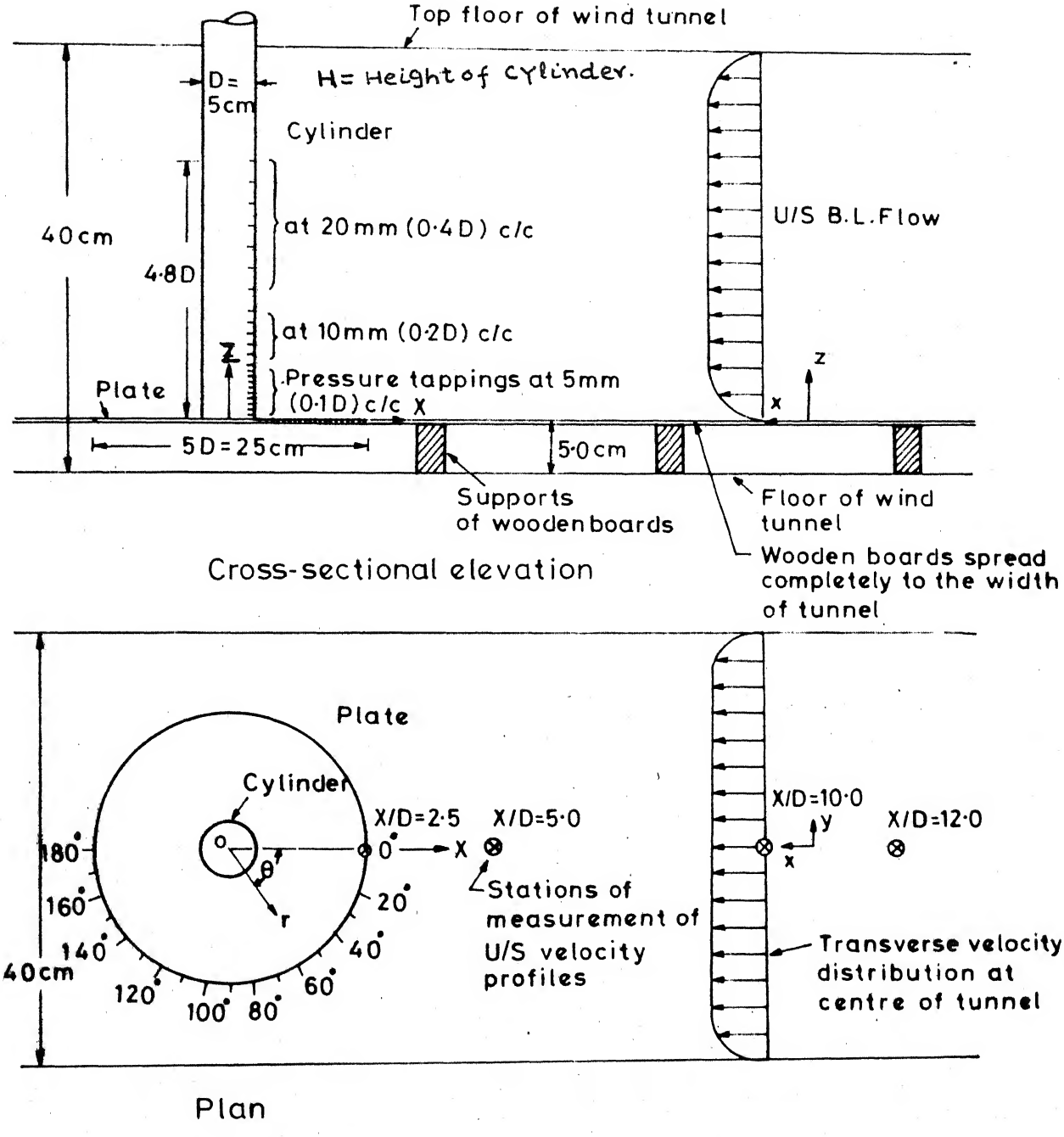

FIG. 2·4 DETAILS OF MODEL IN THE WIND TUNNEL

of width equal to the water flume as described before.

2.4 Measurement of Pressures and Velocity Profiles:

The pressure tubes coming from the pressure tappings on the plate and cylinder are connected to a set of vertical manometers having water. Pressures in terms of depth of water in cm can be read from these manometers. The tunnel pressure is used as a reference pressure. Tunnel pressure has been measured at a distance of 80 cm upstream from centre of the model. The pressures have been measured at each 10^{o} interval from the direction of incoming flow by rotating the model on the wooden board.

The total head tube, having 0.9 mm outside diameter and 5.0 cm length, is used for the measurement of total pressure to determine the velocity profiles. This total head tube is attached to the traversing mechanism which can move in the vertical direction with 0.05 mm least count. The total head probe and static pressure tap hole on the side of the test section are connected to the differential manometer calibrated in inches of water. The velocity profiles have been measured at a distance of 2.5 D, 5.0 D, 10 D and 12 D from the centre of the cylinder and upstream of cylinder along the centre line of the wind tunnel.

The observations for the different sets of boundary layer thickness ranging from 0.47 D to 2.2D have been taken. The boundary layer thickness has been varied either by variation of the free stream velocity or by variation in the roughness of wooden board far upstream from the model. The roughness of the board has been varied by using the mild steel rods on the board far upstream from the model. The temperature of air has also been noted for each set of observations.

2.5 Visualisation Technique:

Visualisation of the flow in the present investigation has been carried out in the water flume. Paint is used as visualisation media. First, the bottom plate and cylinder are painted with different colours and immediately it is kept in water flume, and flow of water is allowed for a sufficient time ranging from 4 to 6 hours. During this time period, the movement of paint takes place leaving flow pattern. Generally two different colours were used, one far upstream of the cylinder and other near the junction of cylinder and plate around the cylinder. The far upstream colour moves with the flow of water towards the cylinder and then it is separated thus forming the line of separation on the bottom plate. The pattern of distribution of paint

near the junction gives the pattern of activities happened inside the separation zone on the bottom plate. The distribution of paint on the surface of cylinder gives the flow pattern such as separation line on the cylinder. The visualisation of flow pattern has been determined for different Froude numbers ranging from subcritical to supercritical flows. Temperature of water has also been noted in each case. After running the flow for nearly 6 hours, the model is taken out of the flume and kept for drying of paints. The flow patterns are traced after the paint has been dried.

CHAPTER III

COMPILATION OF DATA

This chapter deals with the compilation of experimental data. The method for correction of blockage effect on the data is presented. Methods of computing pressure coefficients, drag coefficients, shear velocity and vorticity parameters are presented.

3.1 Blockage Correction Factor:

The flow pattern around the model in the wind tunnel will generally differ from that for the prototype in free stream (i.e. fluid of unlimited extent). There are many tunnel interference effects due to the limited cross-section of the tunnel and also due to blocking of available cross-section due to model. In order to avoid this blockage effect , blockage correction has to be carried out for all the experimental data. This correction is usually carried out by introducing 'Blockage Correction Factor'. There are two types of blockage interference namely:

(a) Solid blockage- involving a change of axial velocity past the model, owing to its partially blocking the flow in the presence of boundary constraints.

(b) Wake blockage - a similar effect due to the reduction of speed within the wake of the model.

If U_F corresponds to the free stream speed (taken to be the speed in the tunnel at the position of the model) and U_T is the tunnel speed, then due to solid blockage effect:

$$U_F = U_T (1 + \epsilon_{sb}) \qquad (3.1)$$

where ϵ_{sb} is blockage correction factor.

In particular, the effect of blockage is to increase the pressure coefficients and drag coefficients from their actual values in free air. Several investigators have studied the effect of blockage. In the present investigation carried out in the wind-tunnel, the following blockage correction factor investigated by O.P.S. Rana (15) has been used, to correct pressure coefficients :

$$\epsilon_s = (1 - \frac{D}{B})^{1.35} \qquad (3.2)$$

where D is the diameter of cylinder, and B is the width of the tunnel. In the present case B = 40 cm, D = 5.0 cm, thus, ϵ_s equals to 0.835.

Blockage correction factor has been used equal to 0.835 to correct measured pressure coefficients in this thesis. This value seems to be high. To estimate the correct blockage correction factor method suggested by Pankhurst is followed. Solid blockage correction ε_{sb} is given for model extending from floor to the roof as

$$\varepsilon_{sb} = \tau \lambda \left(\frac{d}{b}\right)^2 \qquad \text{(Pankhurst)}$$

where $\tau = \frac{\pi^2}{12} = 0.822$, $\lambda = 1.0$ for circular cylinder. 'd' is diameter of cylinder and 'b' is width of the wind tunnel. With d = 5.0 cm and b = 40 cm, ε_{sb} works out to be,

$$\varepsilon_{sb} = 0.012843$$

Wake blockage correction factor according to Pankhurst is,

$$\varepsilon_{wb} = \frac{1}{4} \frac{d}{b} \cdot C_{DT}$$

where C_{DT} is the measured drag coefficient.
Here, form drag coefficient obtained from the surface pressure distribution is used as C_{DT} value. Table 3.1 shows the computation of blockage correction factor.

TABLE 3.1 : COMPUTATION OF BLOCKAGE CORRECTION FACTOR

$\frac{\delta}{D}$	C_D	C_{DT}	ε_{wb}	$\varepsilon_b=\varepsilon_{sb}+\varepsilon_{wb}$	$\varepsilon_s=(1-2\varepsilon_b)$	ε_{cp}
0.47	0.890	1.066	0.0333	0.0461	0.9078	1.087
0.85	0.724	0.867	0.0271	0.0399	0.9202	1.102
0.97	0.813	0.974	0.03044	0.0433	0.9134	1.1457
1.03	0.846	1.013	0.03166	0.0445	0.9110	1.144
1.46	0.746	0.893	0.02791	0.0407	0.9186	1.149
2.20	0.698	0.836	0.02610	0.0389	0.9220	1.151

In Table 3.1, various notations used are,

C_D = average value of drag coefficient corrected for ε_s=0.835

C_{DT}= measured drag coefficient without applying any correction

ε_{wb}= wake blockage correction factor applied to the tunnel velocity

ε_{sb}= solid blockage correction factor applied to the tunnel velocity

ε_b = total blockage correction factor applied to the tunnel velocity

ε_s = blockage correction factor to be applied to the pressure coefficients.

ε_{cp}= correction needed to be applied to the pressure coefficients corrected for ε_s = 0.835.

The values of correction factor (ε_{cp}) given in the last column of Table 3.1 should be multiplied to the pressure coefficients and drag coefficients (corrected for ε_s = 0.835) to get correct values of C_p and C_D.

3.2 Coefficient of Pressure (C_p)

The pressures measured by manometers are reduced to the pressure coefficients (C_p), which are defined as

$$C_p = \frac{P - P_o}{\frac{1}{2} \rho U_o^2} \qquad (3.3)$$

where P is the pressure at the point in the model, P_o is a reference pressure measured far upstream of the model, U_o is the free stream velocity and ρ is the density of air.

In the present investigation, the pressure coefficients have been calculated with respect to the reference pressure measured at a distance of 80 cm from the centre of model. Equation (3.3) gives pressure coefficients without correcting for blockage. Using the blockage correction factor as given in equation (3.2), the pressure coefficients are corrected as

$$C_p = \epsilon_s C_p' \qquad (3.4)$$

where C_p' is the pressure coefficient as given by equation (3.3) and C_p is the corrected pressure coefficient. For further analysis such as calculation of drag coefficients, the corrected C_p will be used.

3.3 Form Drag Coefficients (C_D):

From the corrected pressure coefficients, the local form drag coefficients along the height of cylinder are calculated, using the following relation:

$$C_D = \int_0^{180} C_p \cos\theta \, d\theta \qquad (3.6)$$

The average drag coefficient has been calculated integrating the local drag coefficients over the height of the cylinder,

$$\bar{C}_D = \frac{1}{H} \int_0^H C_D \, dz$$

$$\bar{C}_D = \frac{1}{H} \int_0^H \int_0^{180} C_p \cos\theta \, d\theta \, dz \qquad (3.7)$$

In the present case, the drag coefficients are averaged upto H = 4.8 D.

3.4 Velocity Profiles and Shear Velocity (V_*):

The dynamic head h_v, which is the difference between total head measured by total head tube and wind tunnel static pressure, is recorded in terms of inches of water on a manometer. The velocity of the flow may be converted using usual conversion method, which is simplified as

$$u(m/sec) = 20.162 \sqrt{h_v} \qquad (3.8)$$

where h_v is in inches of water.

The shear velocity V_* ($= \sqrt{\tau_o/\rho}$ where τ_o is the bed shear stress) is calculated assuming the logarithmic velocity distribution namely,

$$\frac{u}{V_*} = \frac{1}{\kappa} \ln y + \text{constant} \qquad (3.9)$$

where y is ordinate measured from the bed, κ is Karman's constant taken equal to 0.4.

3.5 Vortices:

The **lateral vorticity** Ω_y can be defined as,

$$\Omega_y = \frac{1}{2} \left(\frac{\partial u}{\partial z} - \frac{\partial w}{\partial x} \right) \qquad (3.10)$$

For upstream of the model where acceleration of the flow has not started due to cylinder, the transverse velocity 'w' is considered small in comparison to u. Also $\partial w/\partial x$ is small quantity in comparison to $\partial u/\partial z$, the above expression is approximated as,

$$\Omega_y = \frac{1}{2} \frac{\partial u}{\partial z} \qquad (3.11)$$

Non-dimensionalising the vorticity given by equation (3.11), using boundary layer thickness (δ) and shear velocity (V_*), one can get

$$2\Omega_y \frac{\delta}{V_*} = \frac{\delta}{V_*} \frac{\partial u}{\partial z}$$

$$2\Omega_y^* = \frac{\delta}{V_*} \frac{\partial u}{\partial z} \qquad (3.12)$$

where Ω_y^* is non-dimensionalised lateral vorticity. Thus, the vorticity component $\frac{\delta}{V_*} \cdot \frac{\partial u}{\partial z}$ has been analysed from the velocity distribution.

The average vorticity has been calculated integrating the velocity gradients over the boundary layer thickness (δ) as given below,

$$(2\Omega_y^*)_{ave} = \frac{\delta}{V_*} \int_0^{\delta} \frac{\partial u}{\partial z} \, dz \qquad (3.13)$$

The velocity distribution measured at X/D = 5.0 , upstream of the model,has been used for the analysis of vorticity in the upstream boundary layer flow.

3.6 Flow Visualisation:

For the flow visualisation experiments, the flow conditions are expressed in the form of following parameters:

(a) Depth of water ratio = h/D

(b) Froude number = $\frac{U_{ave}}{\sqrt{gh}}$

(c) Reynolds number = $\frac{U_{ave} \cdot D}{\nu}$

(d) Submerged conditions,

where h is depth of flow, D is diameter of the cylinder, U_{ave} is the average velocity of the flow, ν is kinematic viscosity of the fluid.

From the flow patterns obtained by paint impression, following features are observed and then analysed in the Chapter IV.

(a) Separation line on the plate

(b) Separation line along the height of cylinder

(c) Vortex pattern in the separating zone on the plate

(d) Spacing of streaklines observed on the plate at upstream.

CHAPTER IV

RESULTS AND DISCUSSIONS

4.1 General:

This chapter deals with the analysis of results such as flow visualisation, pressure distributions, and drag-characteristics of a cylinder. Firstly, the flow pattern obtained by the paint impression technique has been analysed. With this analysis as a background, the pressure distribution in the separating region has been analysed.

4.2 Flow Visualisation:

Flow patterns by paint impression method in the water flume are obtained for different flow conditions. The sketches of flow patterns for Froude numbers F_r = 0.143 and 1.31 are shown in Figs. 4.1(a), (b). The photographs of the flow patterns for Froude numbers F_r = 0.143, 0.322 and 1.31 are also shown in the Figs. 4.2(a), (b), (c).

4.2.1 Flow Pattern on the Plate:

Regular streak lines of paints are observed on the plate. The average spacing and standard deviation of spacing of streak-lines are given in Table 4.1 for different flow conditions. The streaklines clearly indicate the zone of front stagnation and zone of separation occuring

due to cylinder mounted on the plate. Inside the separating region a number of lines indicating the number of vortices (horse-shoe vortices) are also seen. The streaklines close systematically in the downstream of the cylinder inside the separating zone. The vortices wrap the cylinder on the plate and merge at one point d/s of cylinder shown by the dark portion in Figs.4.1(a),(b) . Thus the streaklines inside the separating region on the plate obtained by paint impression, generally indicate two main vortices of the reverse flow type and two small vortices of opposite sign to the main ones, one between the main ones and the other deep in the junction (corner vortex).

The separation lines on the plate are superposed for different flow conditions as shown in Fig. 4.3 . For supercritical flows , the separating lines do not tend to turn towards the cylinder at the downstream side. For subcritical flows, the separating lines tends to turn towards the cylinder at downstream for fully submerged flow conditions. But, for partially submerged subcritical flow (F_r = 0.322) conditions, complete closure of the separation line just behind the cylinder is observed. In this case free surface effect is predominant and complete closure effect is due to the plunging of vortex from the free-surface at the downstream end.

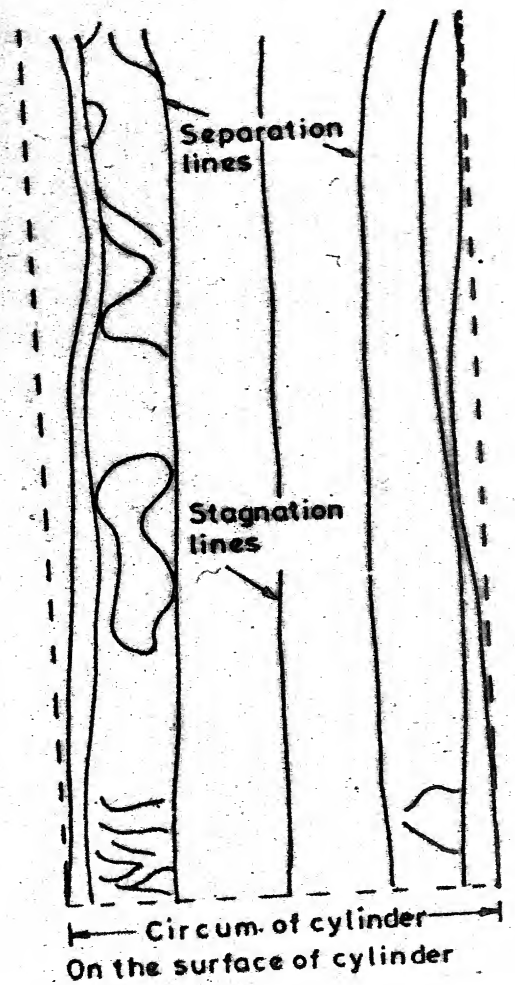

Fully submerged
h/D = 6·72
Fr = 0·143
$Re_D = 0.3 \times 10^3$

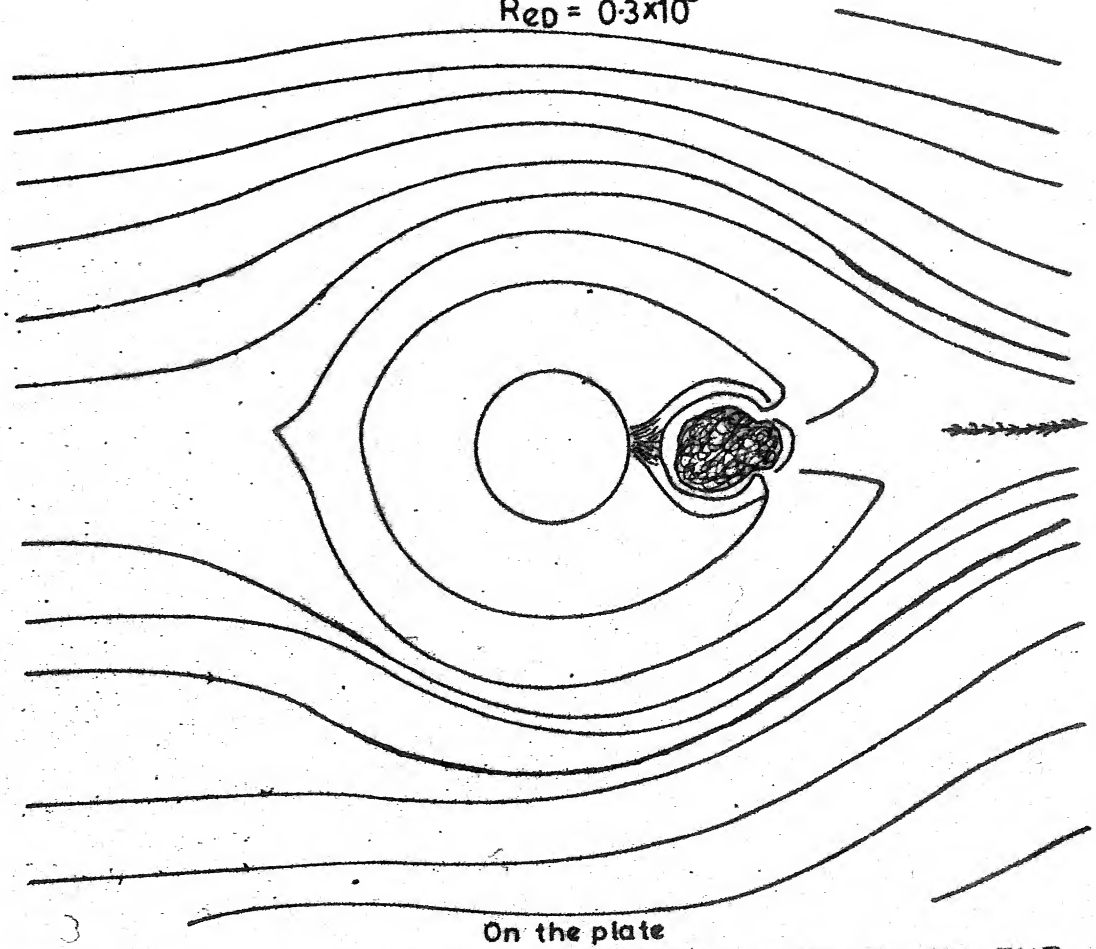

FIG. 4·1 (a) PAINT IMPRESSIONS OF FLOW PATTERN ON THE PLATE AND CYLINDER (Subcritical flow)

Partially submerged

Flow conditions
h/D = 1·78
Fr = 1·31
$R_{eD} = 1{\cdot}48 \times 10^3$

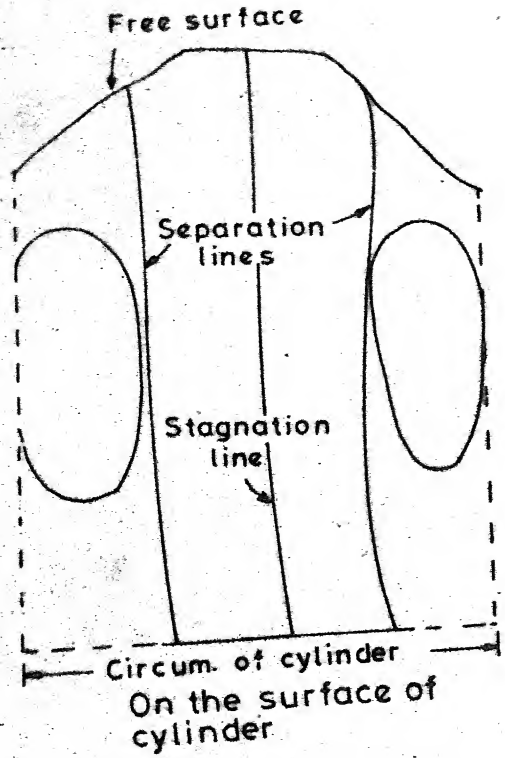

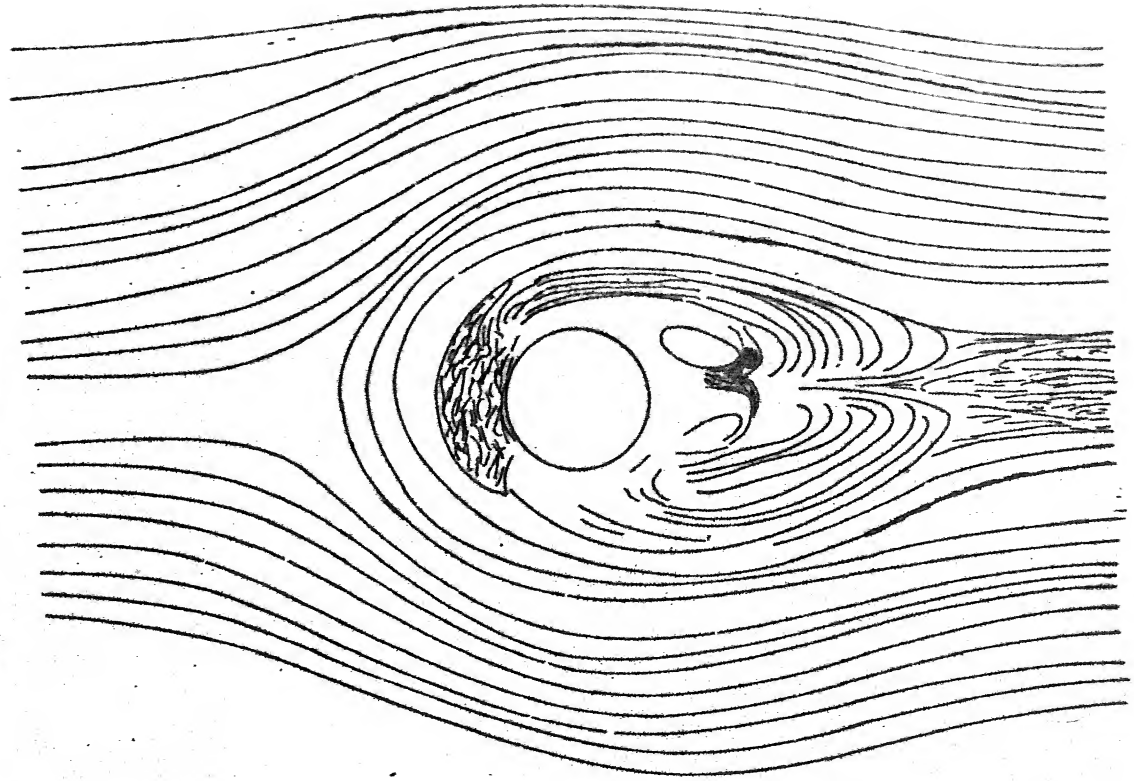

On the plate

FIG. 4·1(b) PAINT IMPRESSIONS OF FLOW PATTERN ON THE PLATE AND CYLINDER (Supercritical flow)

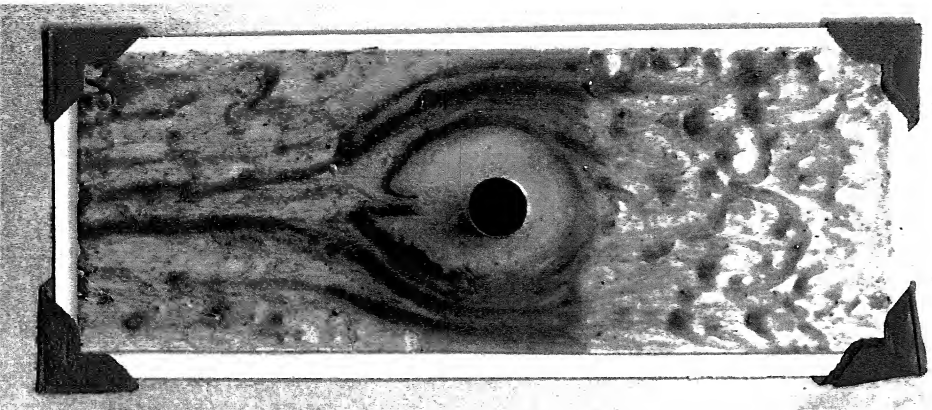

Top View

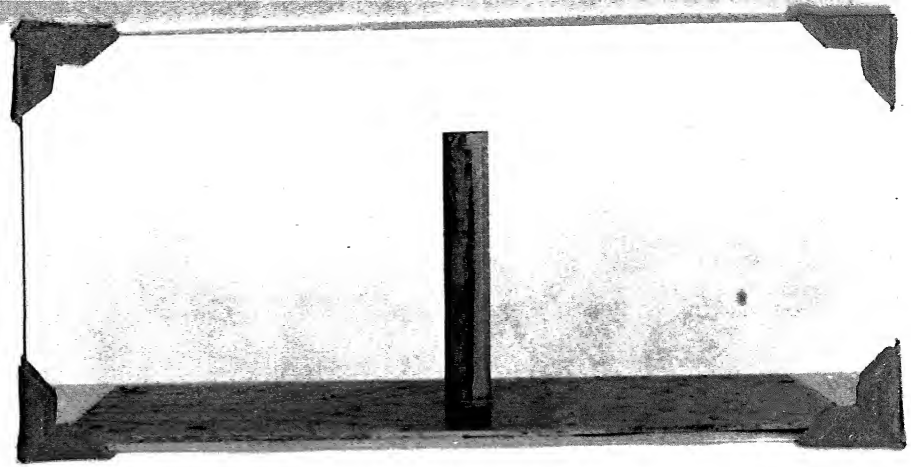

Side View

(a) $F_r = 0.143$

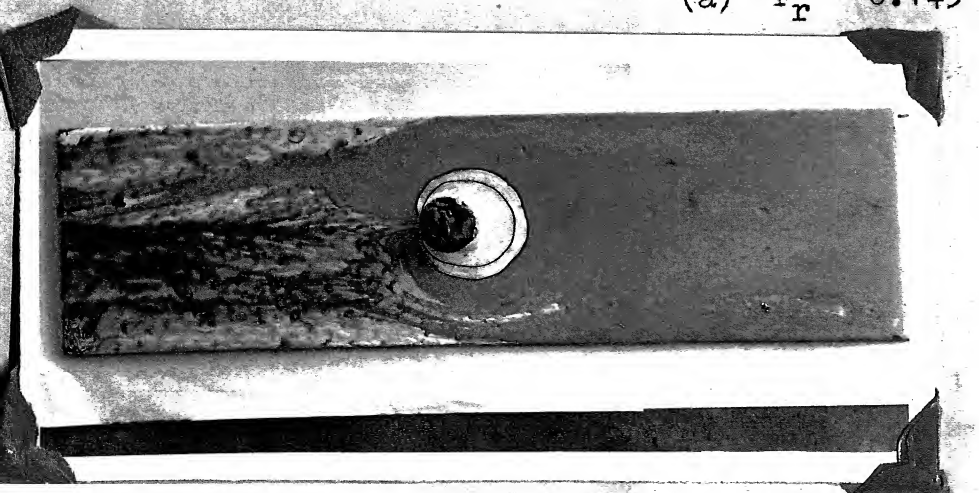

Top View

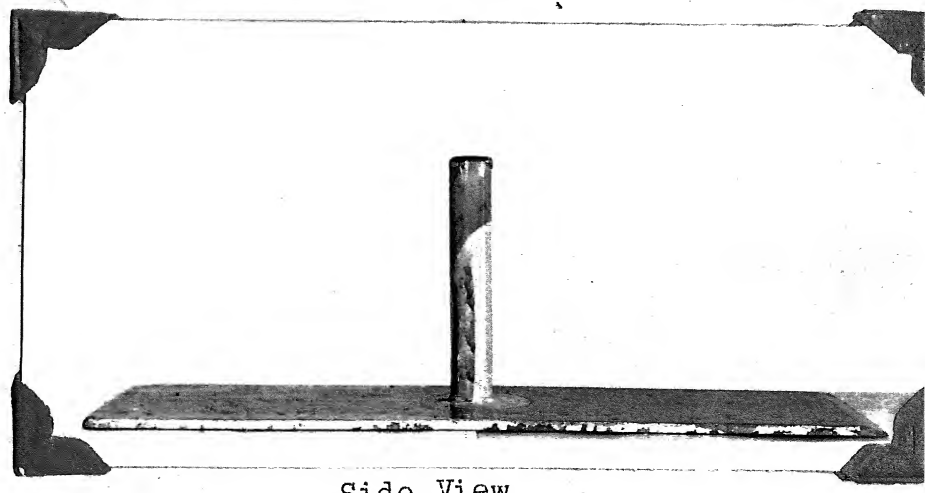

Side View

(b) $F_r = 0.322$

FIG. 4.2 : PHOTOGRAPHS OF FLOW PATTERNS (SUBCRITICAL FLOWS)
(FOR FLOW CONDITIONS, REFER TABLE 4.1)

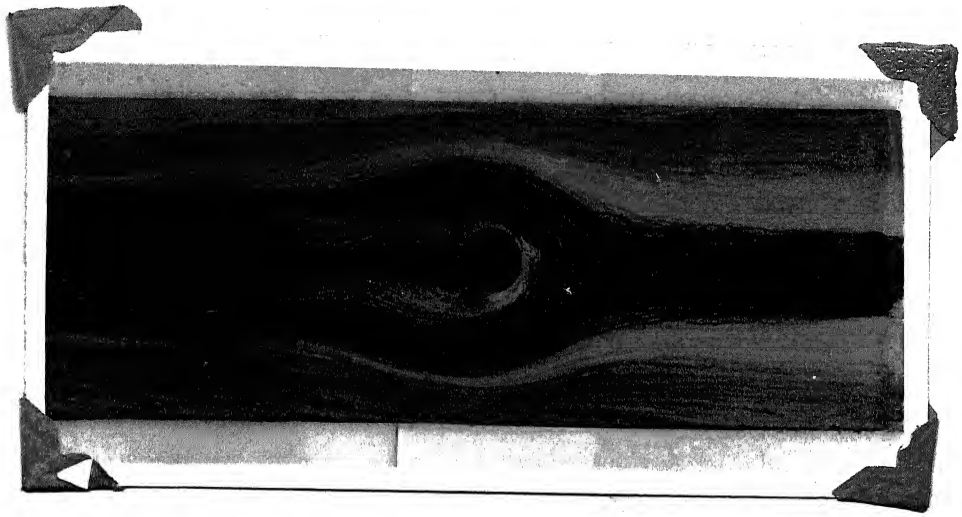

Top View

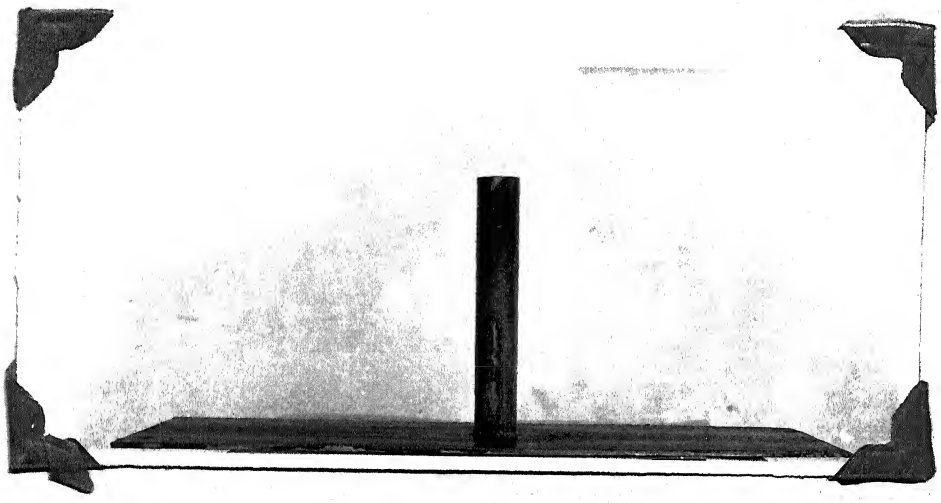

Side View

(c) $F_r = 1.31$

FIG. 4.2 : PHOTOGRAPHS OF FLOW PATTERNS (SUPERCRITICAL FLOWS)
(FOR FLOW CONDITIONS REFER TABLE 4.1)

Notation	$\frac{h}{D}$	F_r	R_{eD}	Submerged conditions
———	6·72	0·143	$0·3 \times 10^3$	Fully
·····	5·60	0·200	0·5	"
—·—·—	3·92	0·322	0·52	Partially
——·——	6·40	0·473	0·95	Fully

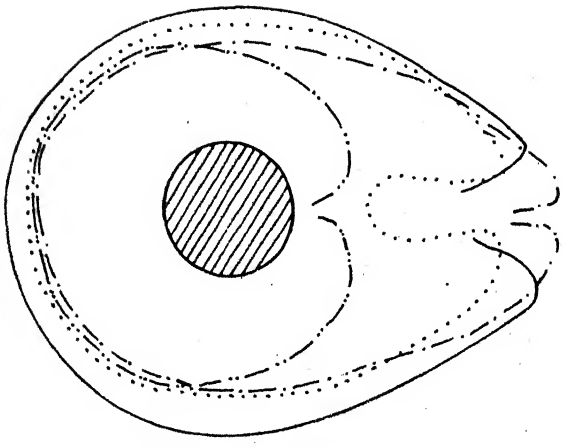

(a) Subcritical flows

Notation	$\frac{h}{D}$	F_r	R_{eD}	Submerged conditions
———	1·78	1·31	1·48	Partially
—·—·—	1·52	1·47	1·45	"

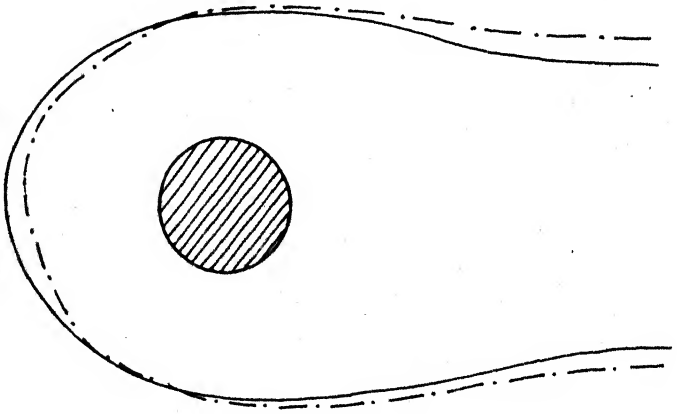

(b) Supercritical flows

FIG. 4·3 PAINT IMPRESSION OF SEPARATION LINES ON THE PLATE FOR DIFFERENT FLOW CONDITIONS

The separating line on the plate is non-dimensionalised as $\frac{a_\theta}{a_o}$, where a_θ is the radial distance measured from the centre of cylinder at angle θ with the direction of flow to the separating line and a_o is the distance of the separation line at $\theta = 0$ from the centre of cylinder. The ratio $\frac{a_\theta}{a_o}$ is plotted against θ for different flow conditions as indicated in the index . The plot of $\frac{a_\theta}{a_o}$ v/s θ for different Froude numbers is shown in Fig. 4.4(b). From the Fig.4.4 (b) one can observe that fully submerged subcritical flows and supercritical flow follow one pattern, whereas, for partially submerged subcritical flow, the curve deviates from the previous ones. This is due to plunging of the vortex from the free surface at the downstream face of the cylinder. The scale a_o/D is plotted against Reynolds numbers ($V_{ave}.D/\nu$) of the flow. Froude numbers are also shown in parantheses. In the subcritical range of Froude number, a_o/D decreases fairly with Reynolds number.

4.2.2 Flow Pattern on the Surface of the Cylinder:

Figures 4.1 (a),(b) show the paint impression of the flow pattern on the surface of the cylinder. The separation line starts just above the plate and continue upto the free surface depending upon the submerged conditions. The stagnation line starting at some distance above the plate

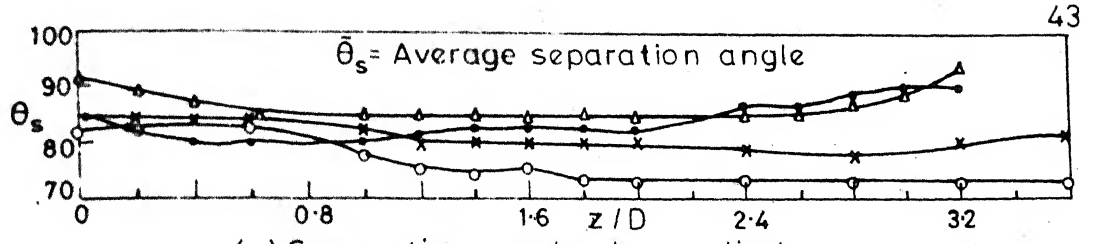

(a) Separation angle along cylinder

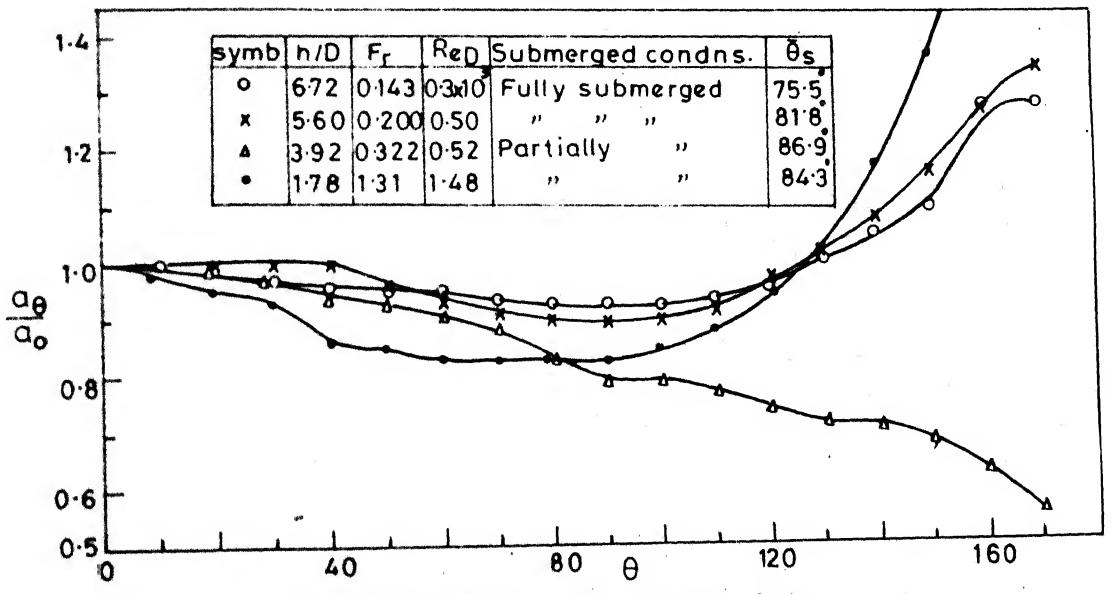

(b) Separation line on the plate

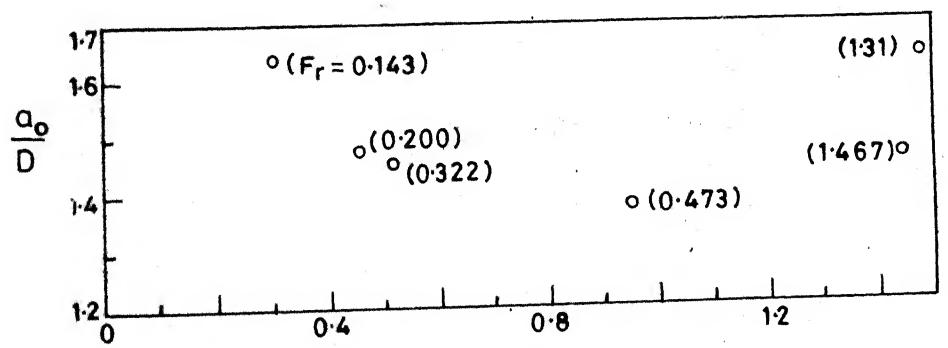

$$R_{eD} = \frac{V_{av}\, D}{\nu} \times 10^3$$

(c) Variation of a_o/D with R_{eD}

FIG. 4·4 PLOT OF SEPARATION LINE ON THE PLATE WITH θ AND SEPARATION ANGLES ALONG THE CYLINDER WITH z/D

at $\theta = 0^{o}$ is observed, in all the cases. Occurrence of vortex centres located symmetrically about the centre line, downstream of the cylinder (near the separation line) is observed. These vortex centres occur near the corner. These vortex centres have also been identified from the pressure contour plots of the cylinder.

The angles of separation line (θ_s) with respect to upstream stagnation line on the cylinder are plotted against Z/D for four flow conditions in Figs. 4.4(a). The value of θ_s vary from 75^{o} to 94^{o} as shown in the figure. The average separation angles for cylinder are shown in Table for different flow conditions in Fig. 4.4(b). The average separation angle ($\bar{\theta}_s$) depends considerably on the submerged conditions and Froude numbers. Generally, $\bar{\theta}_s$, increases with Froude number. But, there is significant increase of $\bar{\theta}_s$ for the partially submerged subcritical flow condition ($\bar{\theta}_s = 86.9^{o}$). This is due to predominancy of free surface as discussed earlier. Table 4.1 show summary of flow visualisation observations.

4.3 Pressure Distributions:

From the data collected from wind tunnel a study on the pressure distributions for the plate and the surface of cylinder is carried out. The contours of constant pressures are plotted. The variation of pressure coefficients

on the plate and around the cylinder with angle θ has also been analysed. The variation of pressure on the plate with r/D at angle θ = 0 is shown, and this variation is related to the vortex pattern inside the separating zone on the plate. Similarly, the pressure contours on the surface of cylinder have also been related to the flow pattern on the surface of cylinder. The effect of boundary layer on the pressure coefficients along the height of cylinder at angle θ = 0, has also been analysed. The analysis of the results of pressure distributions is carried out in the following sections.

4.3.1 Pressure Distributions on the Plate:

(A) Pressure Coefficient Contours:

Figures 4.5(a),(b),(c),(d) show the contours of pressure coefficients on the plate for different boundary layers. The following salient features are observed:

(a) Intense pressure distribution within the separation region where the corner vortex (horse-shoe vortex bent around the cylinder) is observed.

(b) Positive pressure distribution extends upto (±) 40 to 50° on either side near the cylinder.

(c) The maximum negative pressure coefficient occurs at 180° just behind the cylinder.

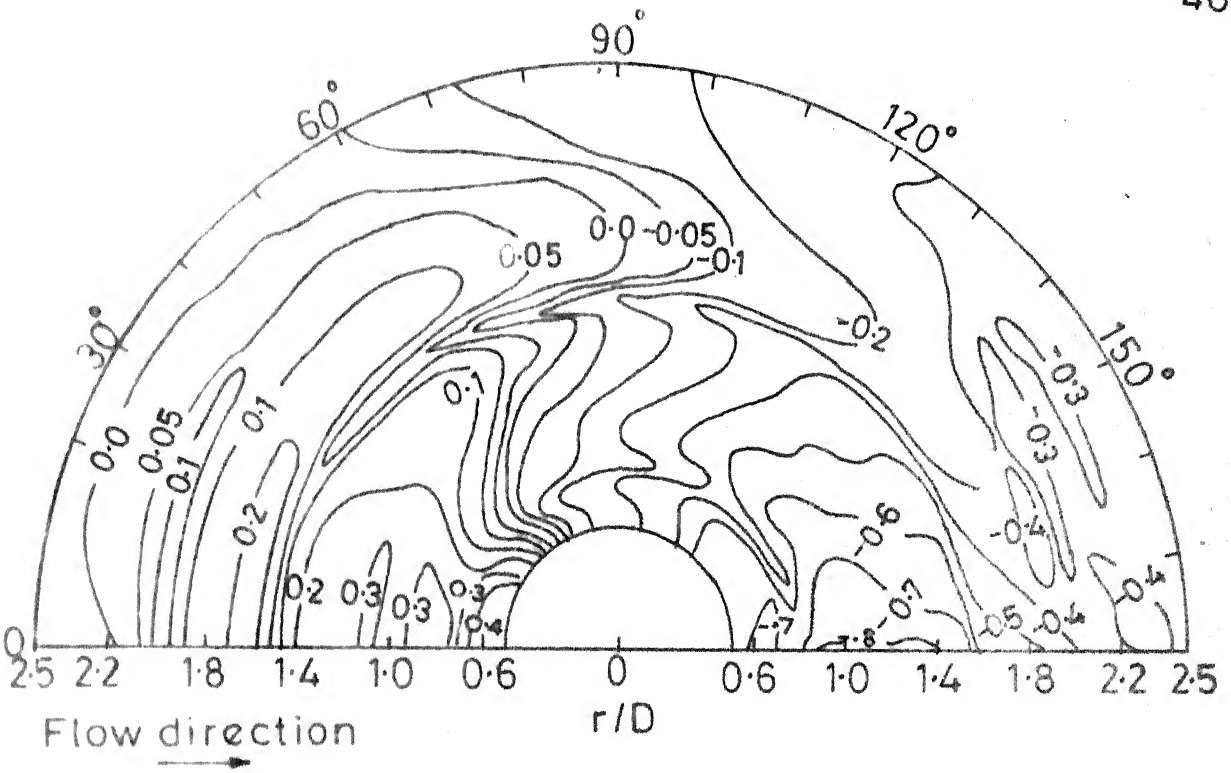

FIG. 4.5(a) CONTOURS OF CONSTANT PRESSURES ON THE PLATE ($\delta/D=0{\cdot}47, R_{eD}=0{\cdot}6\times10^5$)

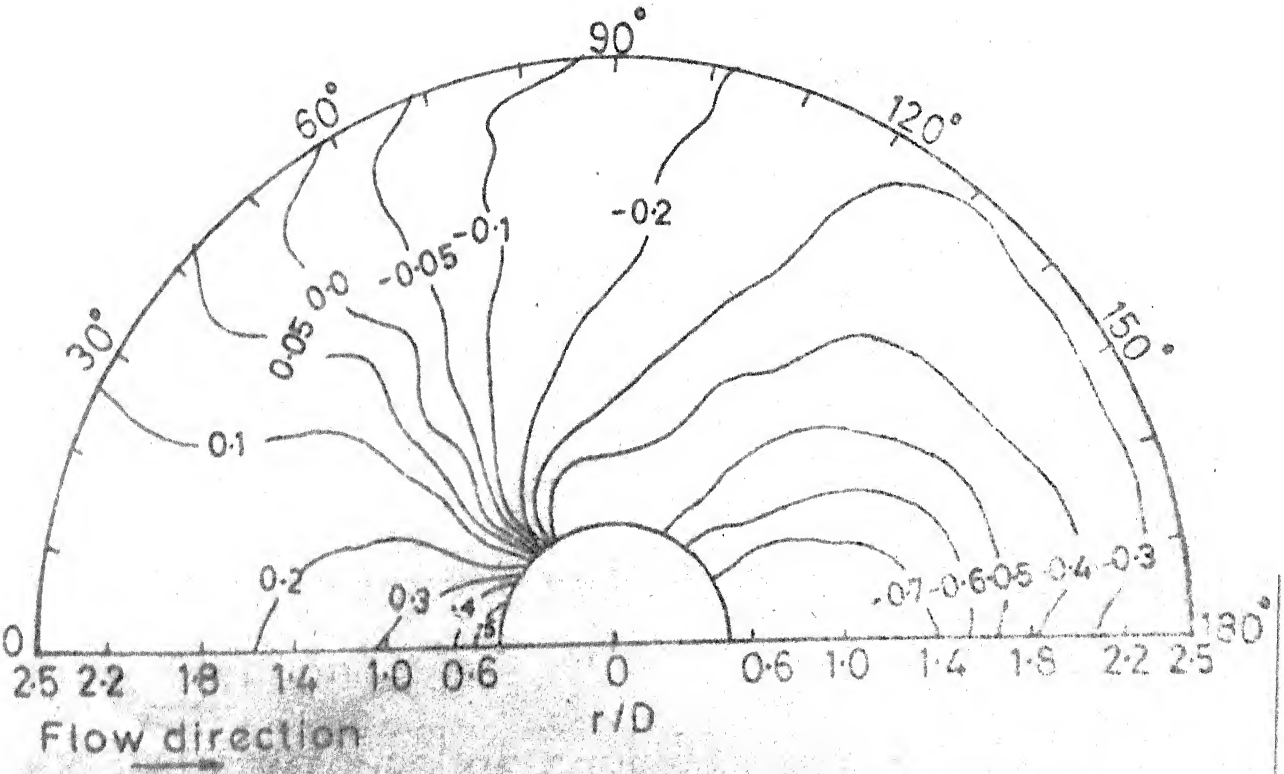

FIG. 4.5(b) CONTOURS OF CONSTAN PRESSURES ON THE PLATE ($\delta/D=1{\cdot}03, R_{eD}=0{\cdot}29\times10^5$)

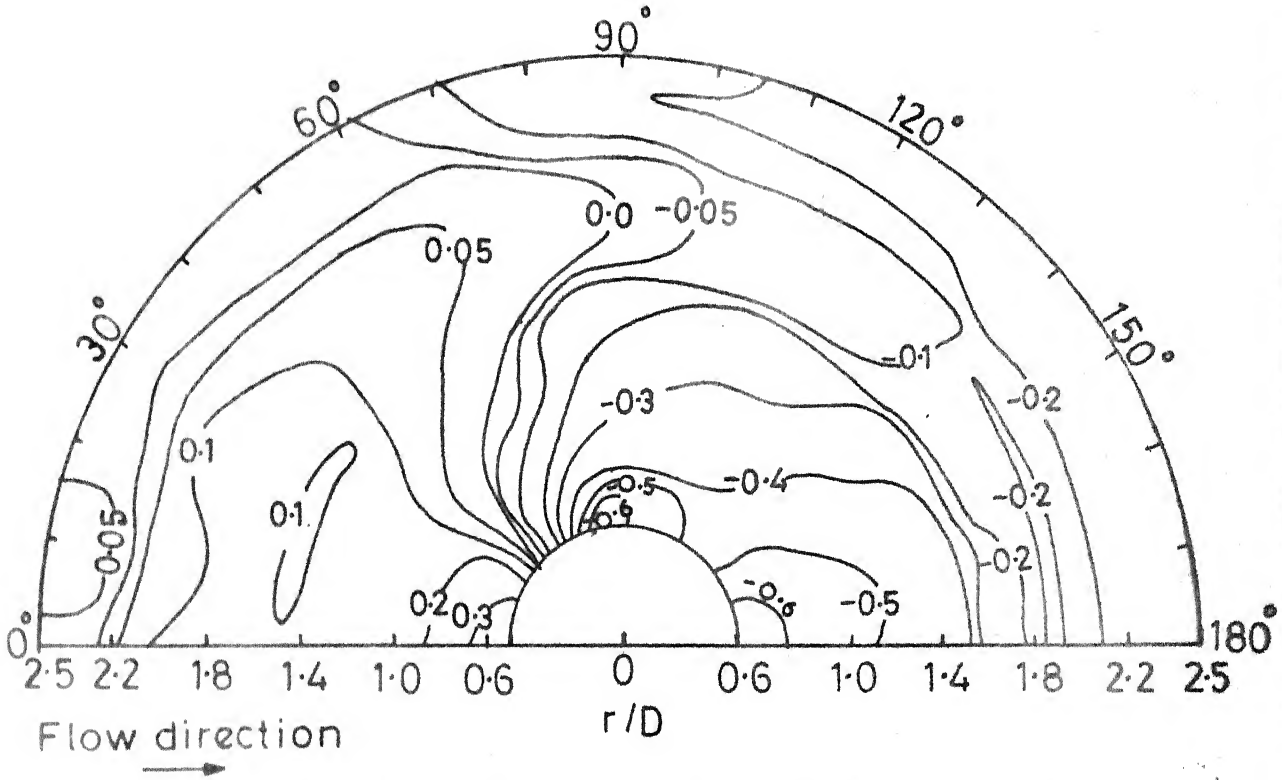

FIG. 4·5(c) CONTOURS OF CONSTANT PRESSURE ON THE PLATE ($\delta/D = 1{\cdot}46$, $R_{eD} = 0{\cdot}630 \times 10^5$)

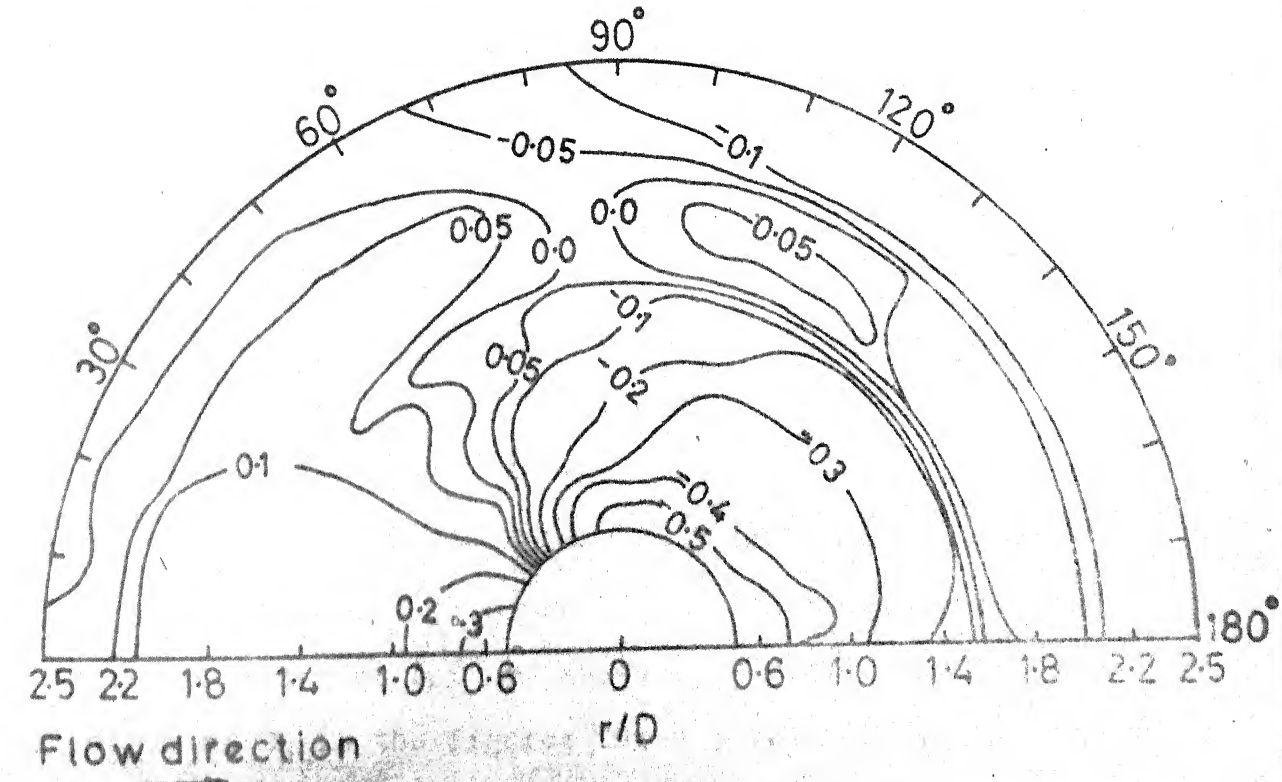

FIG. 4·5(d) CONTOURS OF CONSTANT PRESSURE ON THE PLATE ($\delta/D = 2{\cdot}2$, $R_{eD} = 0{\cdot}645 \times 10^5$)

(d) The maximum positive pressure occurs at 0° at the corner.

(e) For $\delta/D = 0.47$ the lowest pressure (maximum negative) occurs at 180° on the plate in the region extending upto $X = -1.4D$. This is the region of intense vortex behind the cylinder due to merging of incoming upstream vortices.

(B) Variation of Pressure Coefficients with Angle θ:

Figures 4.6(a),(b),(c),(d) show the pressure distribution in terms of C_p with angle θ for different r/D. Following results are observed.

(a) At $\theta = 0$, the pressures are maximum and decrease as θ increases, and become more or less uniform after $\theta > 90^{\circ}$.

(b) The zero pressures occur around $\theta \approx 30$ to 40°.

(c) The pressure coefficient C_p increases with decreasing r/D (approaching the cylinder) at $\theta = 0^{\circ}$.

(d) The positive pressure region is within $(\pm)$ 40° from the centre line.

(C) The Variation of Pressure Coefficients at $\theta = 0^{\circ}$:

The plots of pressure coefficients against r/D at $\theta = 0$, for different δ/D are shown in Fig. 4.7 . The variation of C_p in the figures for $\theta = 0$, indicates systematic

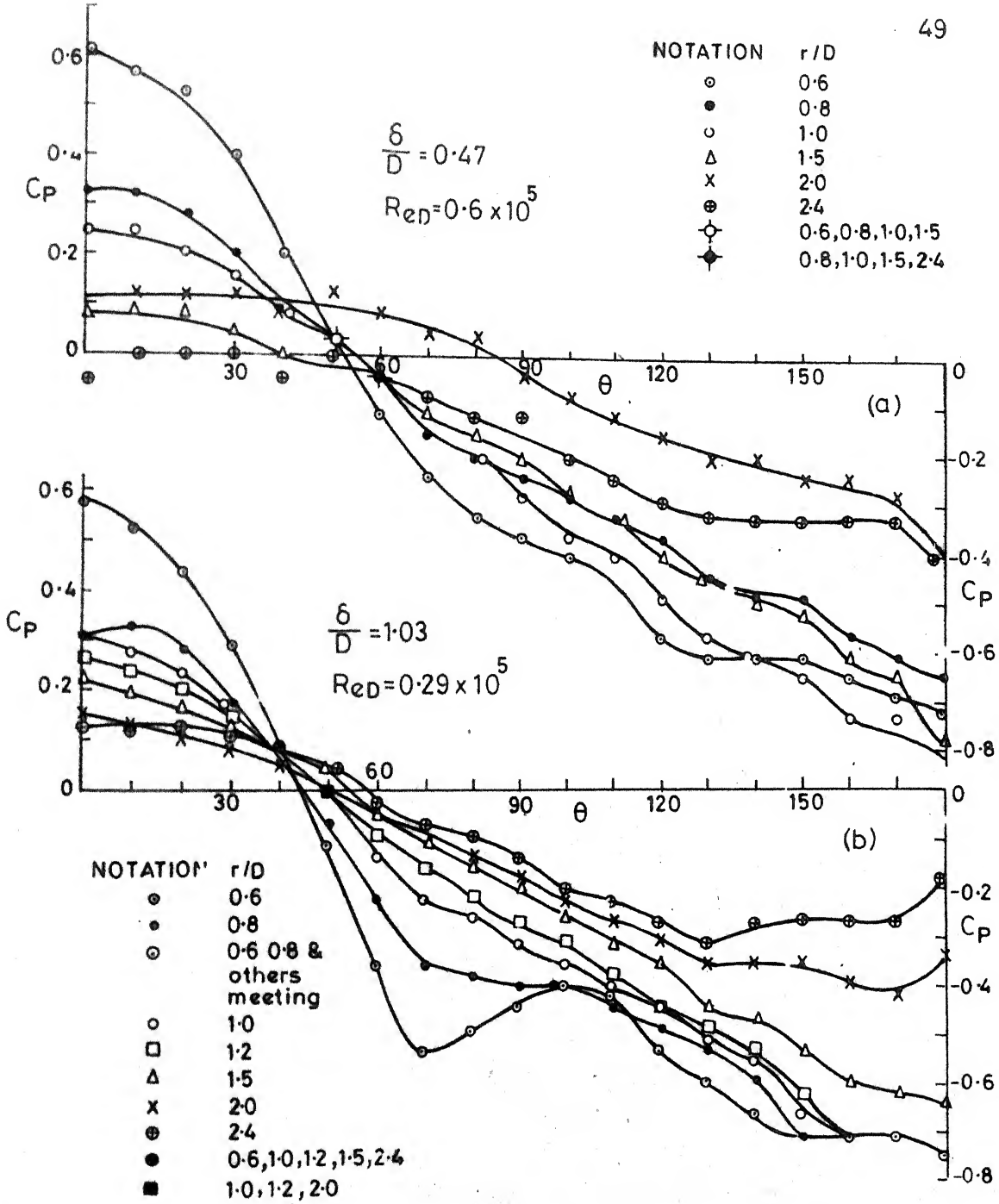

FIG. 4·6 VARIATION OF PRESSURES WITH ANGLE θ FOR PLATE

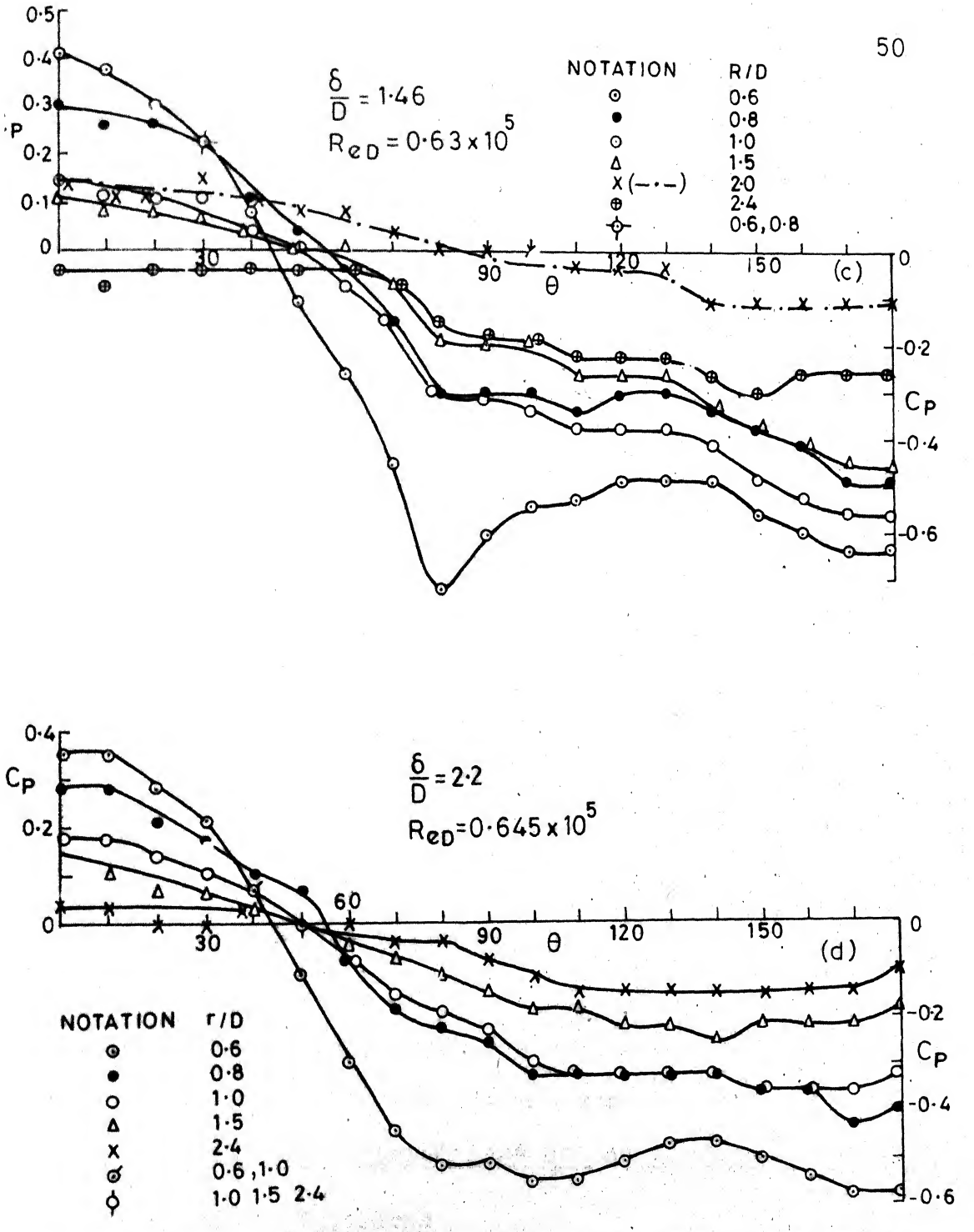

FIG. 4·6 VARIATION OF PRESSURES WITH ANGLE θ ON PLATE

crests and troughs forming valleys which may be considered as possible vortices present in the separating region. There are clearly visible valleys indicating three vortices. The pressure increases gradually from the upstream till the first valley in C_p-curve occurs. This increase in pressure coefficient has one or two small valleys indicating possible vortices in this region. This may be observed in the photograph shown in Fig. 1.1 . Even with the presence of valleys, the pressure gradually increases as r/D decreases and shoots up near the corner (r/D = 0.6). This type of pressure distribution for $\delta/D = 0.47$ for different θ ($\theta = 0$ to 60° at 10° intervals) is shown in Fig. 4.8. The presence of three vortices is clearly observed from this plot. The first major valley occurs at about 1.5 D from the centre of cylinder. From paint impressions, the separating line occurs at around $X/D = 1.5$. This indicates the possibility of separating line occuring around $X/D \approx 1.6$. In Fig. 4.7 possible positions of separation and reattachments of flow due to vortices on the plate from Ref. (18) are shown for comparison of the vortex positioning.

4.3.2 Pressure Distributions on the Surface of the Cylinder:

(A) Pressure Contours:

Contours of constant pressures obtained from the surface pressure distribution for $\delta/D = 0.47, 1.03, 1.46, 2.2$

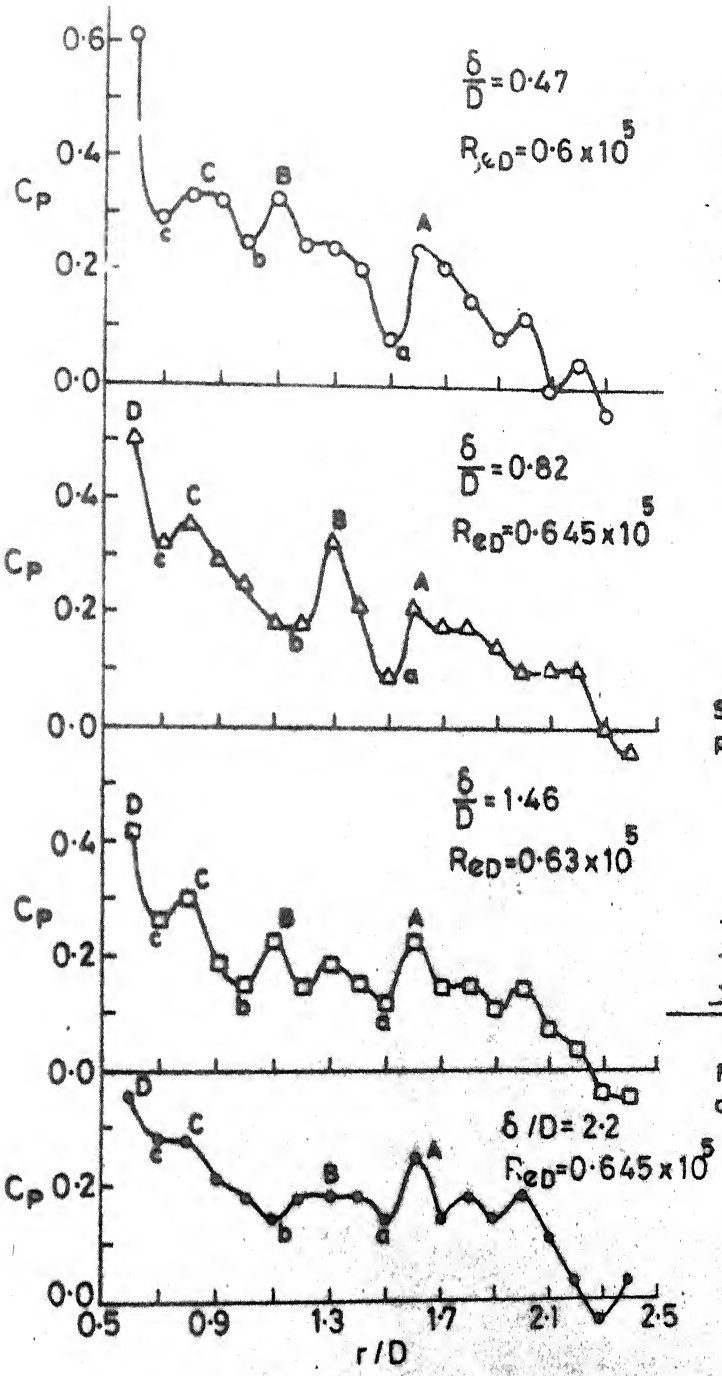

$\Delta C_{P1} = (C_P)_A - (C_P)_a$

$\Delta C_{P2} = (C_P)_B - (C_P)_a$

$\Delta C_{P3} = (C_P)_C - (C_P)_b$

$\Delta C_{P4} = (C_P)_D - (C_P)_c$

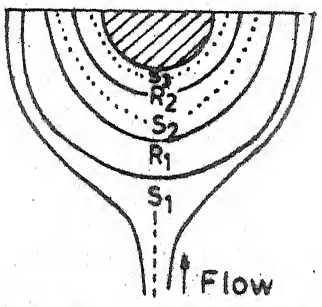

Separation & Reattachment pattern on the plate

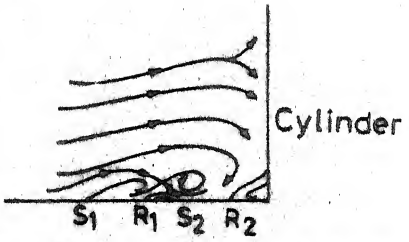

Flow pattern in junction of plate and cylinder (Ref. 18)

FIG. 4·7 PRESSURE DISTRIBUTION ALONG θ=0 ON THE PLATE FOR DIFFERENT δ/D VALUES

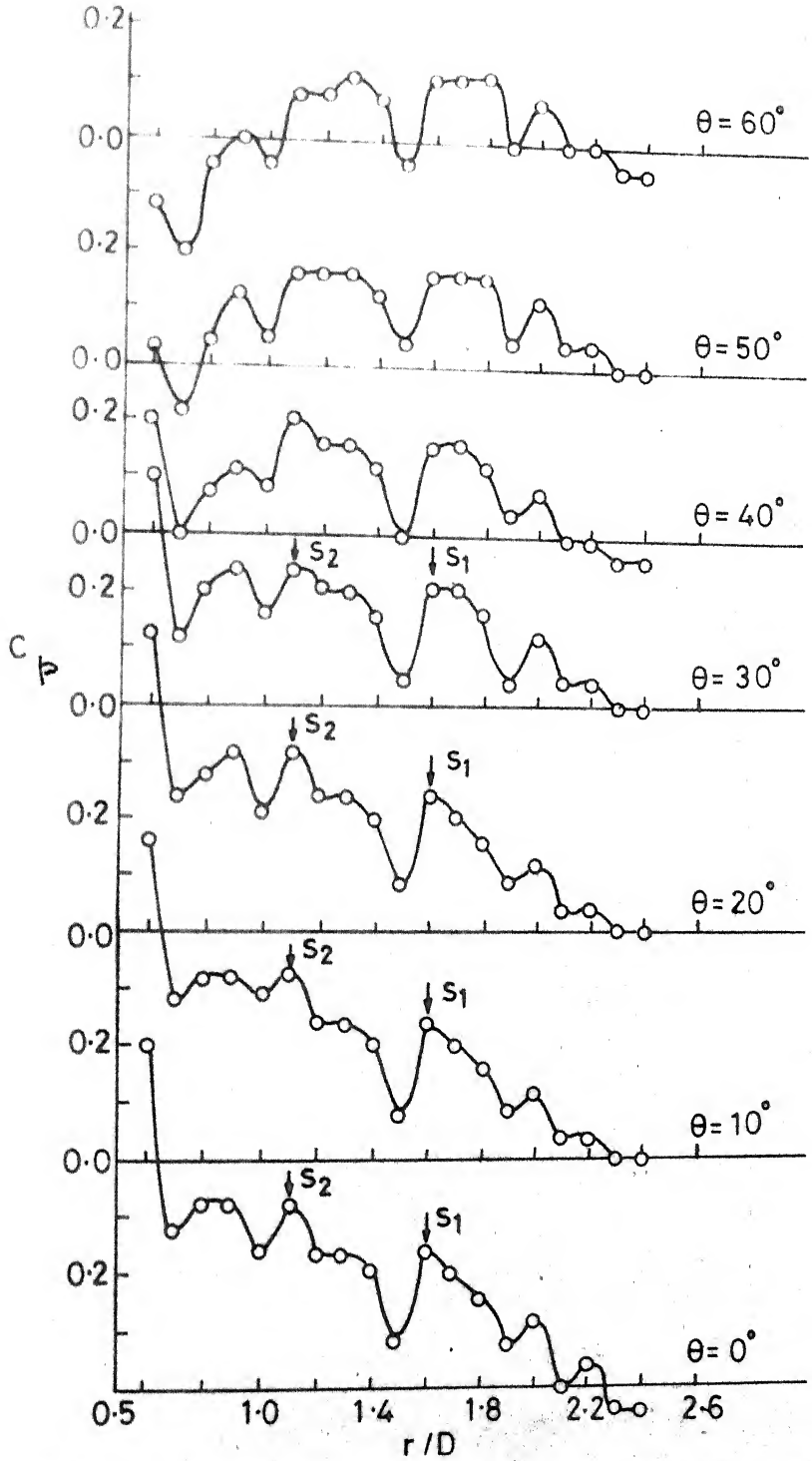

FIG·4·8 PRESSURE DISTRIBUTION ON THE PLATE FOR DIFFERENT θ FOR δ/D = 0·47

are shown in Figs.4.9(a),(b),(c),(d). The following results are observed from these contours:

(a) The pressure contours are gradually increasing at $\theta = 0$ from the junction of the plate to approximately the edge of boundary layers.

(b) The pressure above the boundary layer depth remains fairly constant at $\theta = 0$.

(c) The contour of zero pressure occurs around $\theta = 40^{\circ}$.

(d) The spacing of contours upto around $\theta = 30^{\circ}$ is large, which indicates the gradual decrease in pressures, with θ upto around 30°. In general, the spacing of contours decreases gradually from $\theta = 0^{\circ}$ to $\theta = 70^{\circ}$ or 80°, thus indicating that the rate of decrease of pressures increases with angle θ upto 70° or 80°. The separation line also occurs at angles between 70° and 80°. Thus, it is concluded that there is a rapid decrease in the pressures with θ till the separation occurs.

(e) There is a systematic pressure distribution observed from $\theta = 0^{\circ}$ to the possible separation line. In the separation zone , (after separation line), no systematic pressure distribution is observed.

(f) There are two regions of the lowest pressures around 80° within the boundary layer, indicating the possibility of vortex centre. The lowest vortex will be occuring due to the corner. This is observed in all

the pressure contours. The counter vortices within the boundary layer are observed for all cases except $\delta/D = 1.03$. The presence of corner vortex is also observed in flow visualisations.

(g) Also, the lowest pressure region occurs around $\theta=80^{\circ}$ at a height of 3.6 to 4.0 D. This indicates the possible region of vortex shedding. Vortices are believed to shed at this height (9).

(h) Pressure contours are lifted up around 80° to 90° indicating that the vortex may be sucked up in the wake, and minimum C_p indicates the possible position at which the vortex shedding from the cylinder occurs.

(B) <u>The Variation of Pressure Coefficients with Angle θ around the Cylinder:</u>

The coefficient of pressure C_p is plotted against angle θ for different Z/D values in the Figs.4.10(a),(b),(c),(d) $\delta/D = 0.47, 1.03, 1.46, 2.2$, respectively. Following points are noticed from these figures.

(a) The positive pressure field occurs within $\pm 40^{\circ}$ and negative pressure field in the remaining region.

(b) In the positive pressure region pressure coefficient increases from the junction of the plate within the boundary layer and remains fairly constant outside the boundary layer.

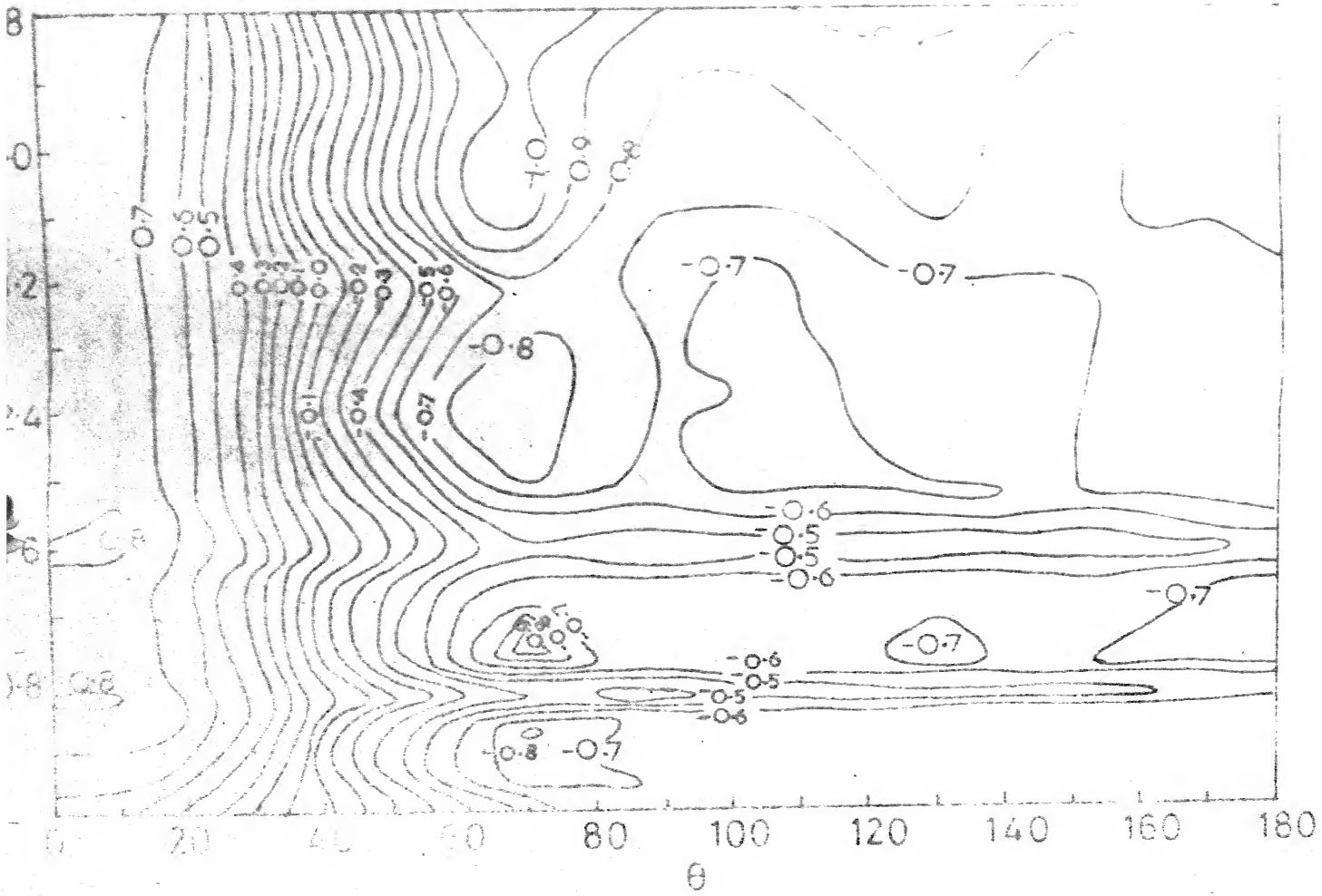

FIG. 4.9(a) CONTOURS OF CONSTANT PRESSURES ON THE SURFACE OF CYLINDER ($\delta/D = 0{\cdot}47$, $R_{eD} = 0{\cdot}6 \times 10^5$)

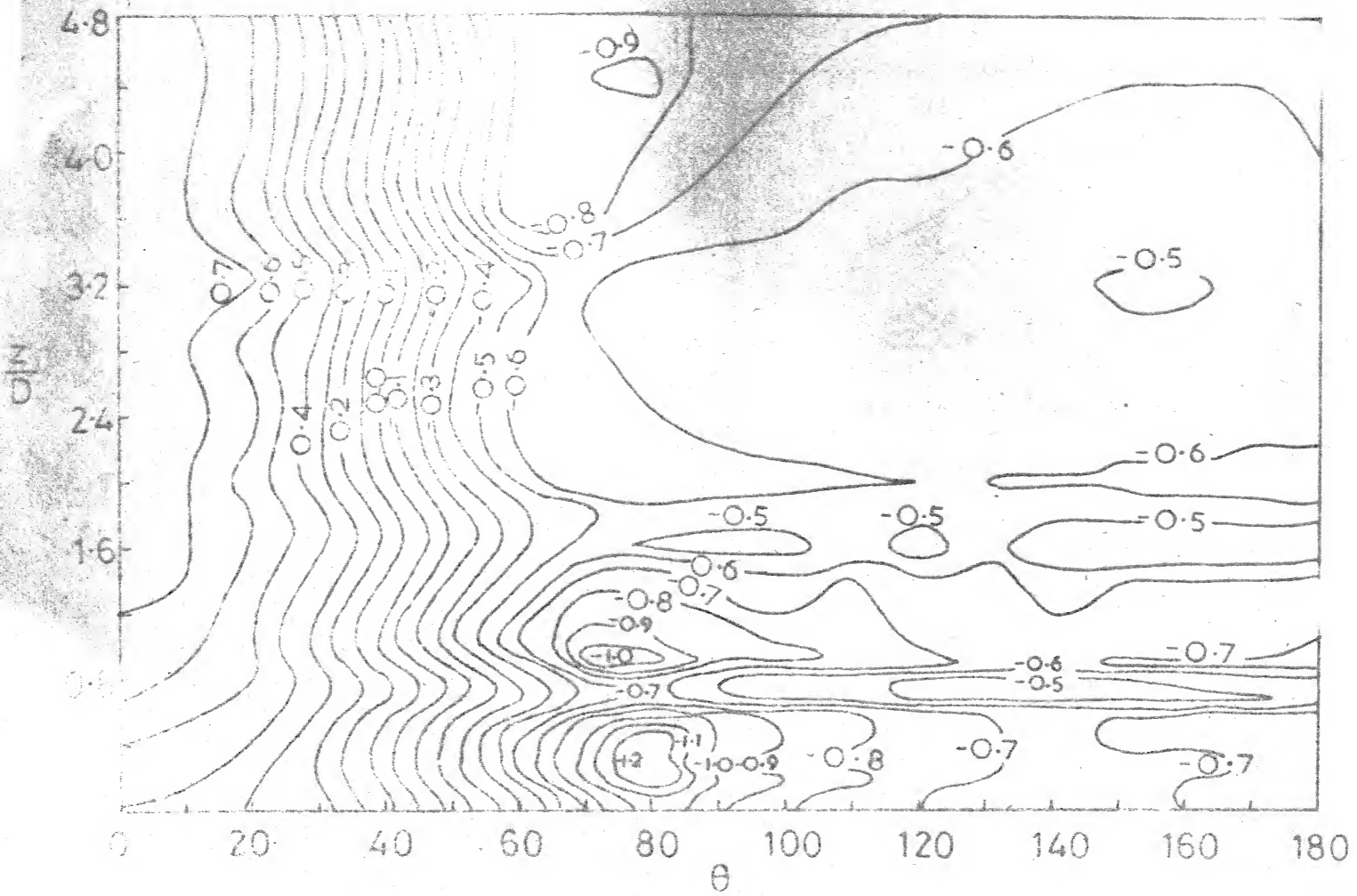

FIG. 49(c) CONTOURS OF CONSTANT PESSURES ON THE SURFACE OF CYLINDER ($\delta/D=1{\cdot}46, Re_D=0{\cdot}63\times10^5$)

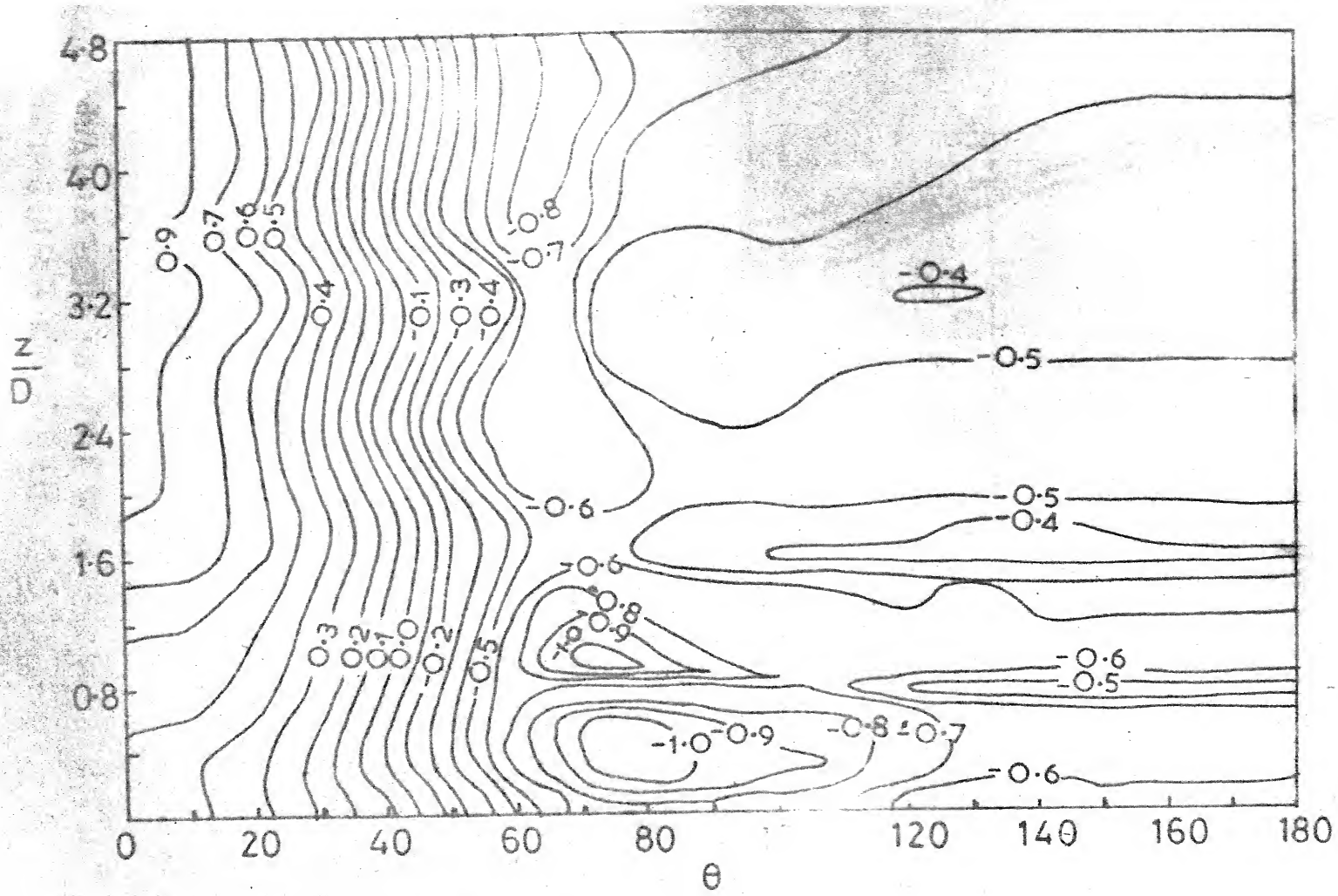

FIG. 4.9(d) CONTOURS OF CONSTANT PRESSURES ON THE SURFACE OF CYLINDER ($\delta/D = 2.2, R_{eD} = 0.645 \times 10^5$)

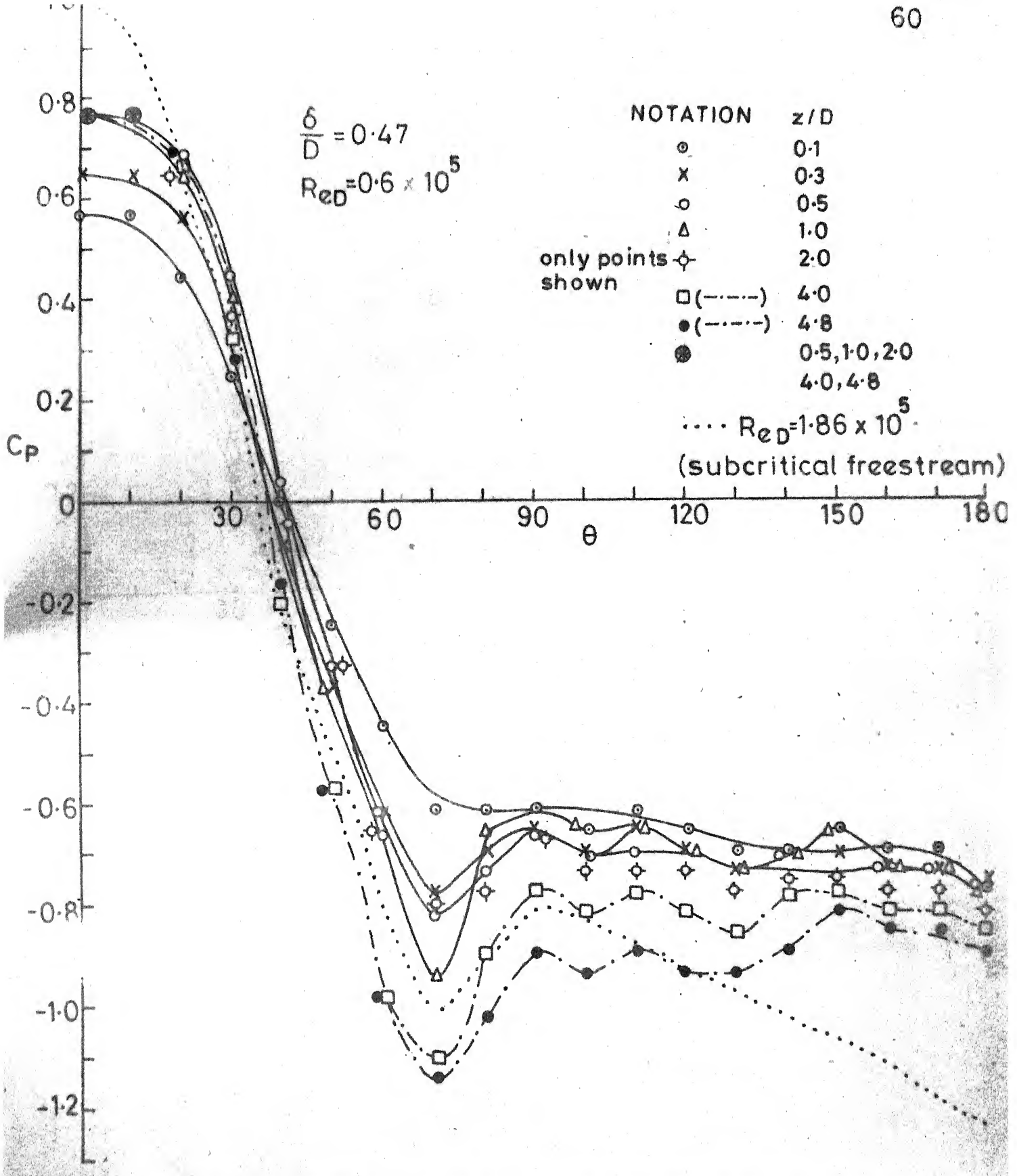

FIG.4.10(a) VARIATION OF PRESSURES WITH ANGLE θ AROUND CIRCULAR CYLINDER

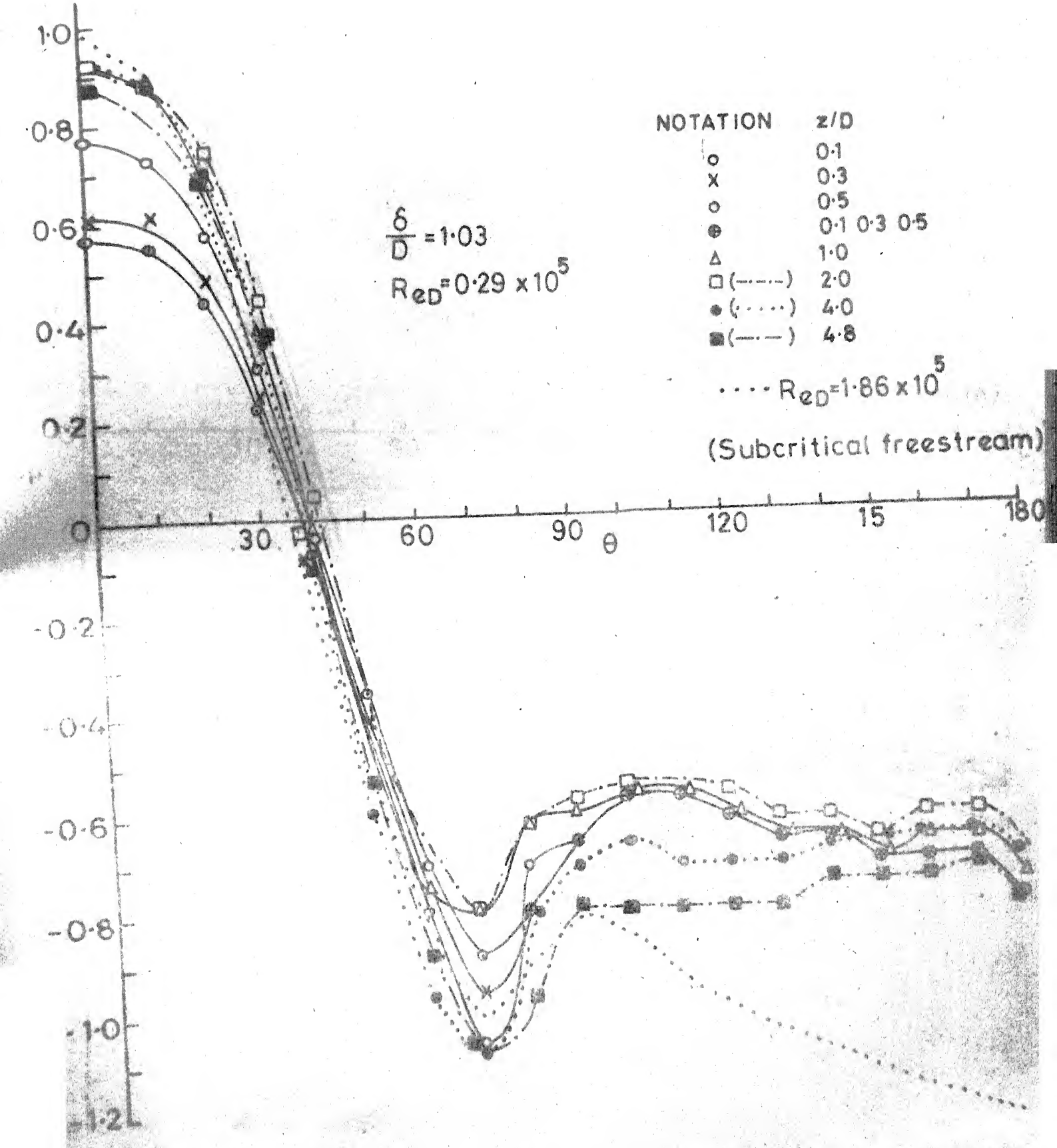

FIG·4·10(b) VARIATION OF PRESSURES WITH ANGLE θ AROUND CIRCULAR CYLINDER

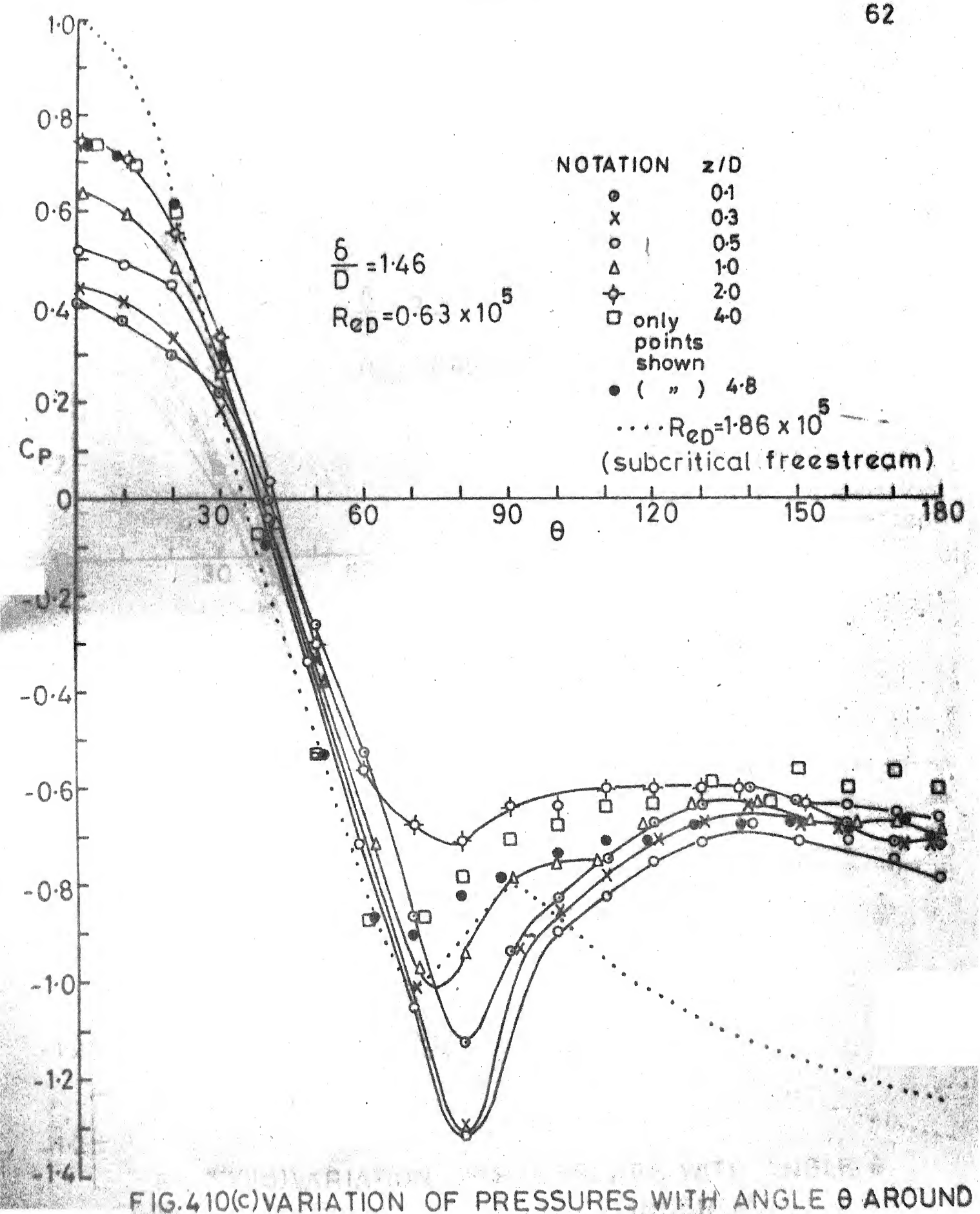

FIG. 4·10(c) VARIATION OF PRESSURES WITH ANGLE θ AROUND CIRCULAR CYLINDER

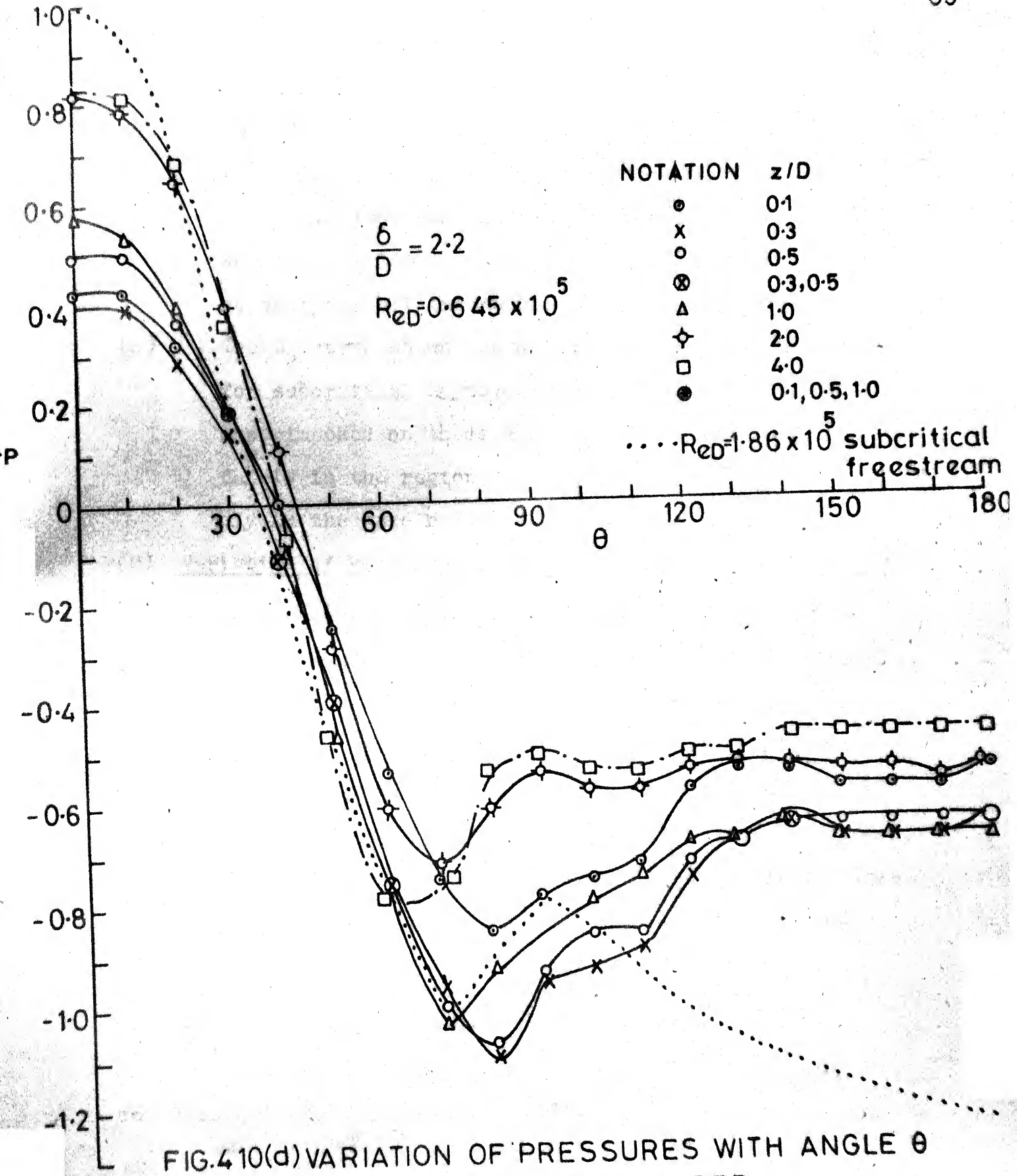

FIG.4 10(d) VARIATION OF PRESSURES WITH ANGLE θ AROUND CIRCULAR CYLINDER

(c) The minimum pressure coefficients occur between 70° to 80° where the region of separation begins.

(d) The pressure decreases rapidly from $\theta = 0^{\circ}$ to $\theta = 70\text{-}80^{\circ}$, and gradually pressure recovery takes place from $\theta \simeq 70^{\circ}$ to 100° and then remains fairly constant in the wake region ($\theta \geq \pm 100^{\circ}$) . This variation can be seen for all the cases.

(e) The C_p curve shown as dotted line taken from Ref. (19) for subcritical Reynolds number in free stream is superimposed on these curves. This curve agrees fairly in the region $0 \leq \theta \leq 90^{\circ}$ but deviates considerably in the wake region.

C) Variation of Pressures Along the Height of the Cylinder at $\theta = 0$ with Boundary Layer Effect:

The pressure coefficients at $\theta = 0$ (C_{po}) are plotted against Z/δ for four boundary layers $\delta/D = 0.47$, 0.82, 1.46, 2.2, in Fig.4.11. It is observed that pressure coefficient C_{po} increases gradually from $C_{po} \simeq 0.4$ (near the junction of plate) to $C_{po} \simeq 0.8$ till the edge of boundary layer is reached, and remains fairly constant outside the boundary layer. This clearly indicates that the pressure recovery occurs within the boundary layer region.

4.4 Vortices in Upstream Boundary Layer Flow:

Considering w and $\partial v/\partial x$ as small quantities, in comparison to $\partial u/\partial z$, **lateral vorticity** Ω_y is approximated as

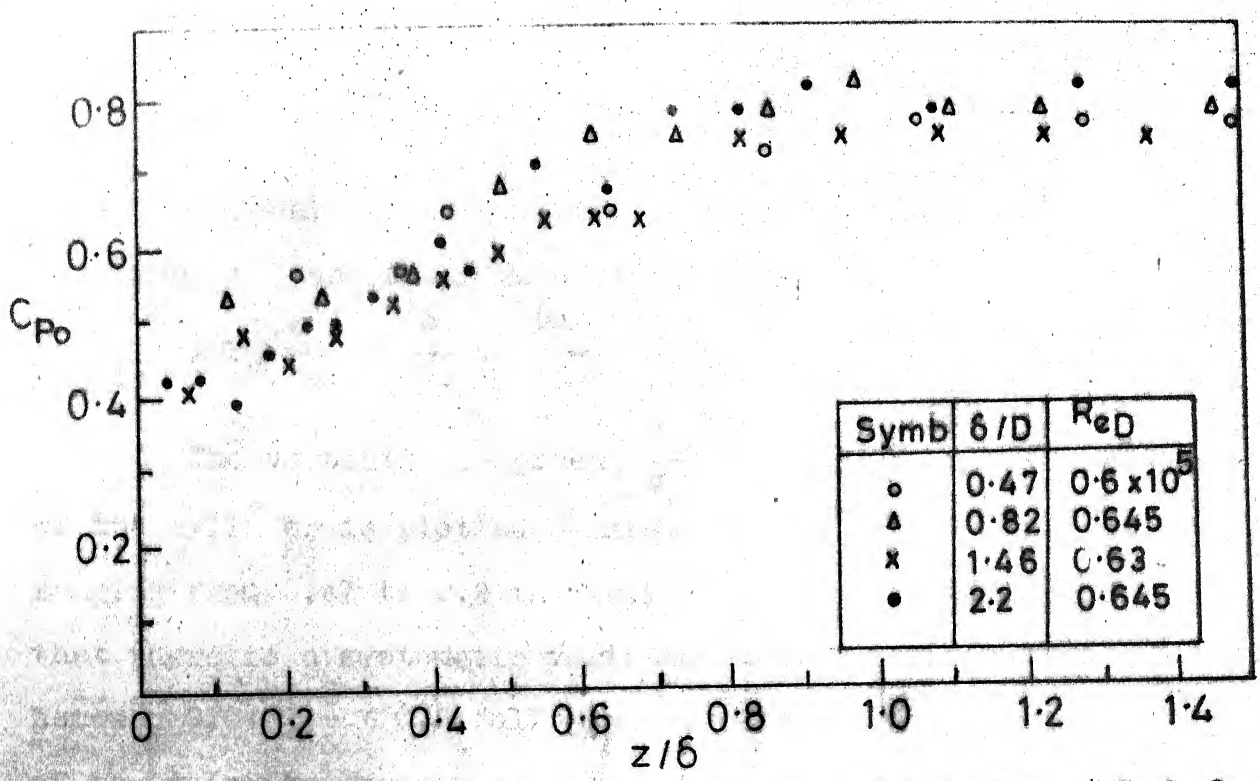

FIG.4.11 VARIATION OF PRESSURE COEFFICIENT AT θ=0 (C_{Po}) ALONG THE HEIGHT OF CYLINDER w.r. TO B.L. THICKNESS

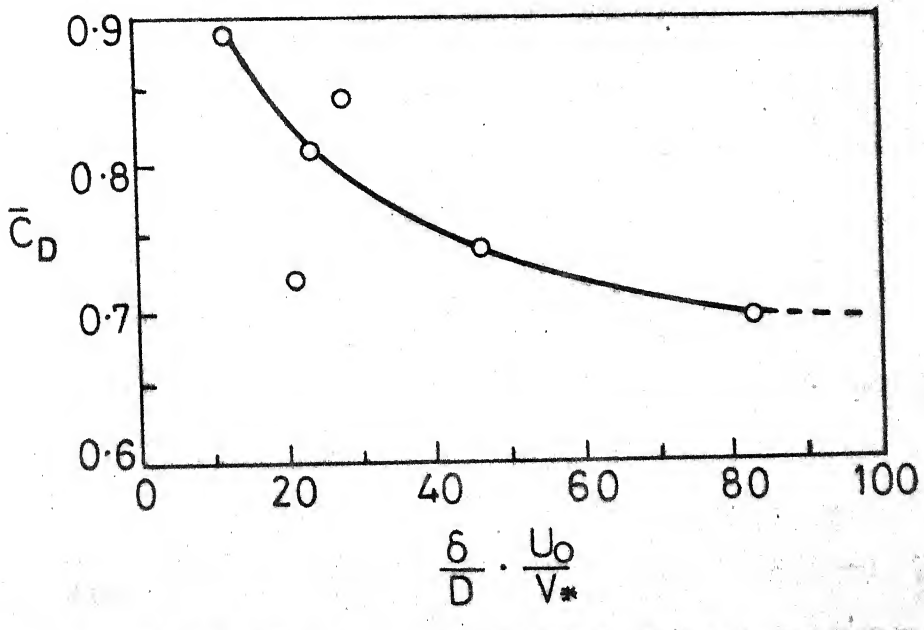

FIG.4.12 VARIATION OF AVERAGE DRAG COEFFICIENT WITH PARAMETER $(\delta/D)\cdot(U_o/V_*)$

$$\Omega_y = \frac{1}{2} \cdot \frac{\partial u}{\partial z} \qquad (4.1)$$

Non-dimensionalising the vorticity using boundary layer thickness (δ) and shear velocity (V_*) as

$$2\Omega_y \frac{\delta}{V_*} = \frac{\delta}{V_*} \cdot \frac{\partial u}{\partial z} \qquad (4.2)$$

The vorticity component $\frac{\delta}{V_*} \frac{\partial u}{\partial z}$ for $x/D = 5.0$ upstream of the cylinder is plotted against Z/δ for four δ/D ratios ranging from 0.47 to 2.2 in Fig.4.13 . It may be observed that there is a systematic variation in logarithmic zone between $0.01 \leq \frac{Z}{\delta} < 0.2$ following logarithmic distribution of the velocity, namely

$$\frac{\delta}{V_*} \frac{\partial u}{\partial z} = \frac{1}{\kappa} \frac{\delta}{Z} \qquad \text{where } \kappa = 0.4 \qquad (4.3)$$

The magnitude $\frac{\delta}{V_*} \frac{\partial u}{\partial z}$ in the outer region (velocity defect law) is very small and with large scatter.

An expression for vorticity distribution for the zone near the wall (Viscous zone), assuming that both turbulent and laminar shear stresses are present, can be written as

$$\frac{\tau_o}{\rho} = \nu \frac{\partial u}{\partial z} + \kappa^2 z^2 \left(\frac{\partial u}{\partial z}\right)^2 \qquad (4.4)$$

Non-dimensionalizing with δ and V_* and writing for vorticity, one can get following expression

$$\frac{\delta}{V_*} \frac{\partial u}{\partial z} = \frac{1}{2\kappa^2} \frac{1}{\delta^{+2}} \left(\frac{\delta}{z}\right)^2 \pm \frac{1}{2\kappa^2} \sqrt{\left\{ \frac{1}{\delta^{+2}} \left(\frac{\delta}{z}\right)^4 + 4\kappa^2 \left(\frac{\delta}{z}\right)^2 \right\}} \qquad (4.5)$$

where $\delta^+ = \frac{V_* \delta}{\nu}$

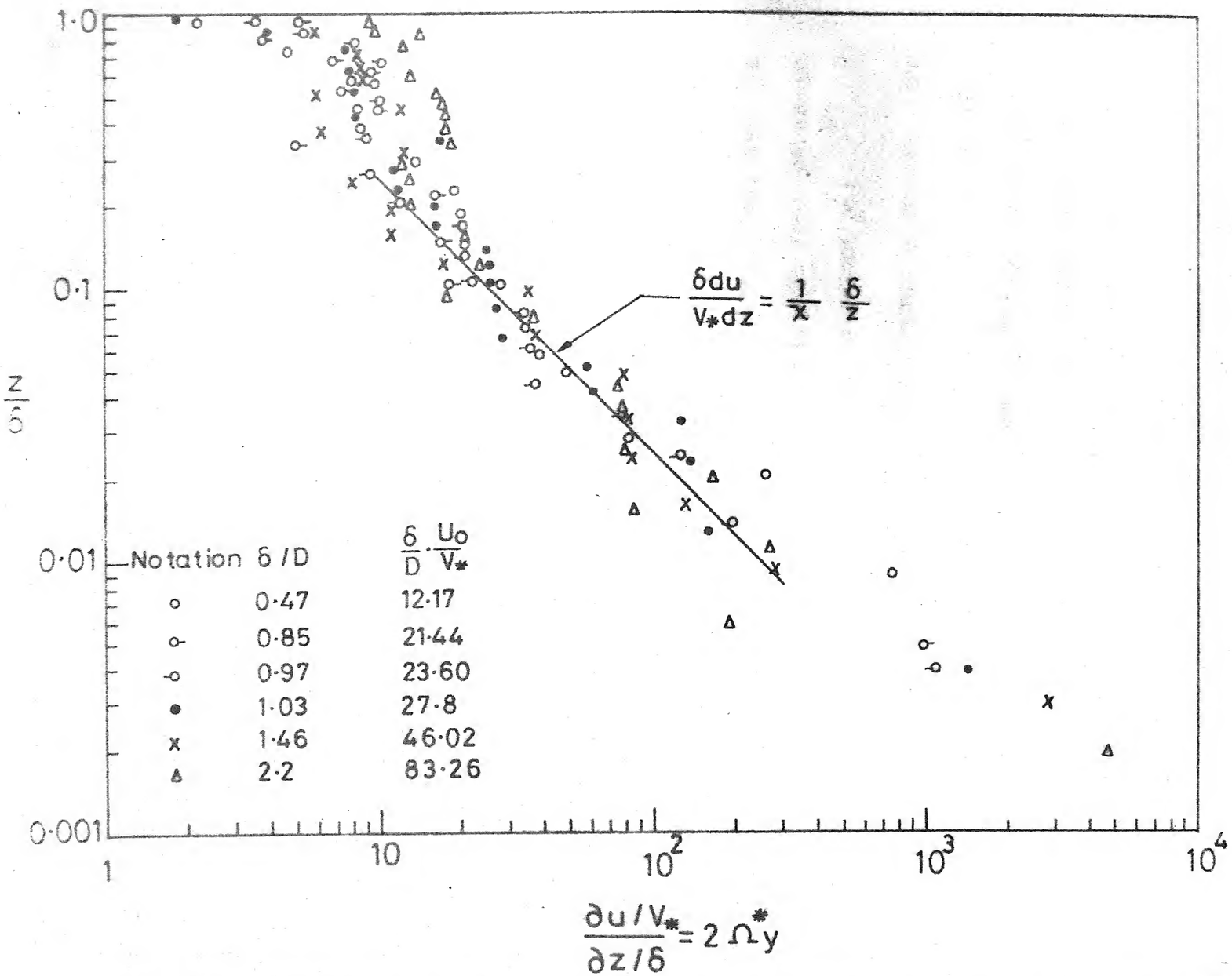

FIG. 4·13 DISTRIBUTION OF NON DIMENSIONALISED VORTICITY ($2\Omega^*_y$) WITHIN THE BOUNDARY LAYER

This expression simplifies as equation (4.3) for the logarithmic zone, where $z/\delta > 0.01$.

4.4.1 Distribution of Average Vorticity:

The vorticity component $\frac{\delta}{V_*}\frac{\partial u}{\partial z}$ is averaged over the boundary layer thickness at x/D = 5.0 and this average value works out to U_o. This can be written in terms of δ, D and V_* as $\delta/D.U_o/V_*$ and is designated as vorticity parameter. For further analysis $\frac{\delta}{D}\frac{U_o}{V_*}$ is taken as a parameter.

The pressure coefficient C_p on the plate for $\theta = 0$ averaged over the distance x/D from 0.6 to 2.4 is plotted against the parameter $(\frac{\delta}{D}\frac{U_o}{V_*})$ in Fig. 4.14(c.). The value of average C_p is found to remain fairly constant with the parameter $\frac{\delta}{D}\frac{U_o}{V_*}$. The maximum pressure coefficient on the plate at $\theta = 0$ which occurs near the corner (at $\frac{x}{D} = 0.6$) is plotted against the parameter $(\frac{\delta}{D}\frac{U_o}{V_*})$ Fig. 4.14(b). It is observed that the maximum C_p fairly decreases with $\frac{\delta}{D}\frac{U_o}{V_*}$. The difference in pressure coefficient of trough and crest (valley), is a function of the strength of vortex. This difference for three valleys are given in Table 4.3 for different $\frac{\delta}{D}\frac{U_o}{V_*}$ values. The magnitudes of ΔC_{p1}, ΔC_{p2} and ΔC_{p3} decrease with the parameter $\frac{\delta}{D}\frac{U_o}{V_*}$. ΔC_{p4} which gives the increase of pressure near the corner is also given in the Table 4.3. Here ΔC_{p1}, ΔC_{p2}, ΔC_{p3} are difference in pressure coefficients between crest and trough as shown in Fig. 4.7.

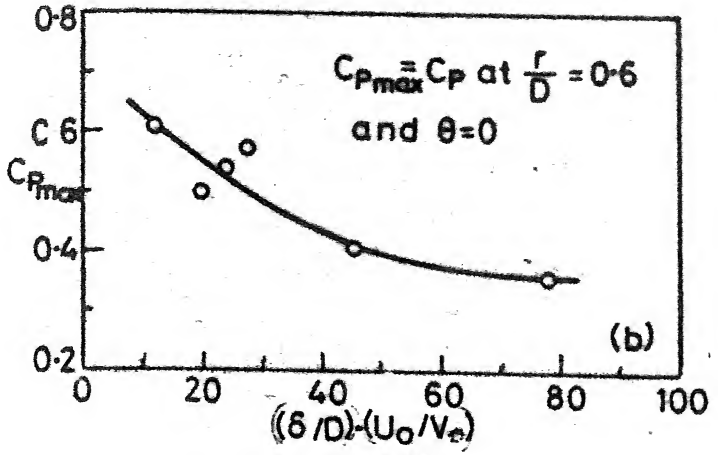

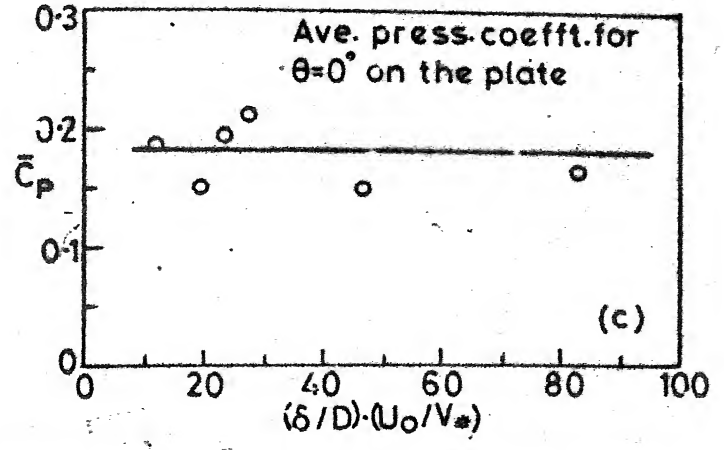

FIG. 4.14 VARIATION OF MAXIMUM PRESSURE COEFFICIENT & AVERAGE PRESSURE CO-EFFICIENT ON THE PLATE WITH PARAMETER $(\delta/D)\cdot(U_0/V_*)$

4.5 Distribution of Drag Coefficient C_D for the Cylinder:

First, local drag coefficients (C_D) are calculated along the height of the cylinder and its variation along the height is observed. Then average drag coefficient $\bar{C}_D$ is analysed with the parameter $(\frac{\delta}{D} \frac{U_o}{V_*})$.

4.5.1 Variation of Local Form Drag Coefficients (C_D) Along the Height of Cylinder:

The local form drag coefficient C_D is plotted against z/D for different δ/D values in Fig. 4.15 . The drag coefficient increases with z/D till the depth approximately equals the boundary layer thickness and then decreases gradually and remains fairly constant in the region outside boundary layer. The sharp crest of the maximum C_D is observed in lower values of δ/D and gradual smoothening of crest takes place for large δ/D values. The magnitude of C_D in the region outside boundary layer varies from 0.7 to 0.9 which is very much less in comparison to the drag coefficient of the cylinder held in the free-stream for corresponding range of Reynolds numbers.

4.5.2 Average Value of Form Drag Coefficient:

The form drag coefficient ($\bar{C}_D$) averaged upto z/D = 4.8 is plotted against the parameter $\frac{\delta}{D} \frac{U_o}{V_*}$ in Fig. 4.12 . The magnitude of average drag coefficient ($\bar{C}_D$) decreases with increase in $\frac{\delta}{D} \frac{U_o}{V_*}$ as shown in Fig. 4.12.

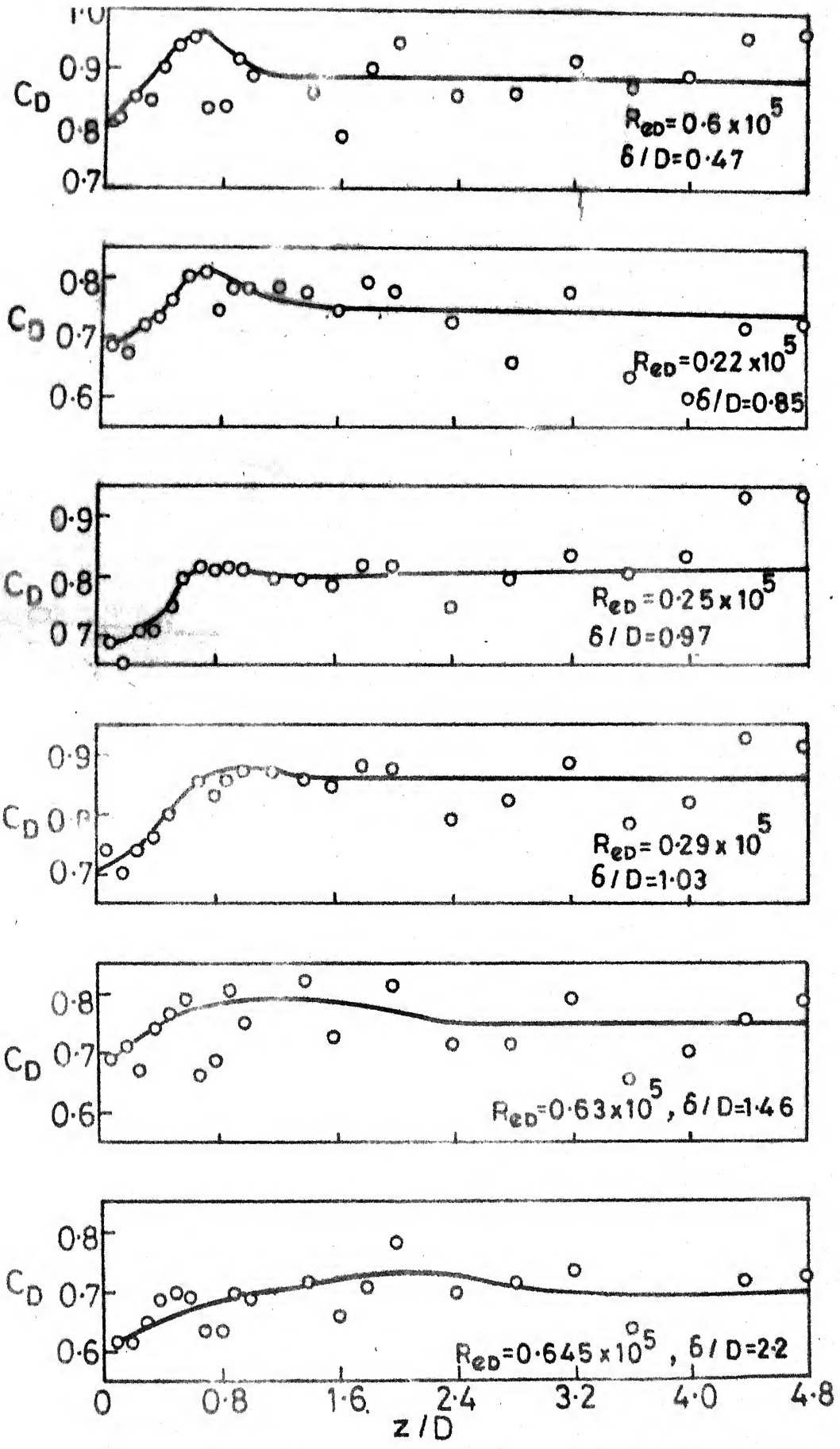

FIG. 4·15 VARIATION OF LOCAL DRAG COEFFICIENTS ALONG THE HEIGHT OF CYLINDER

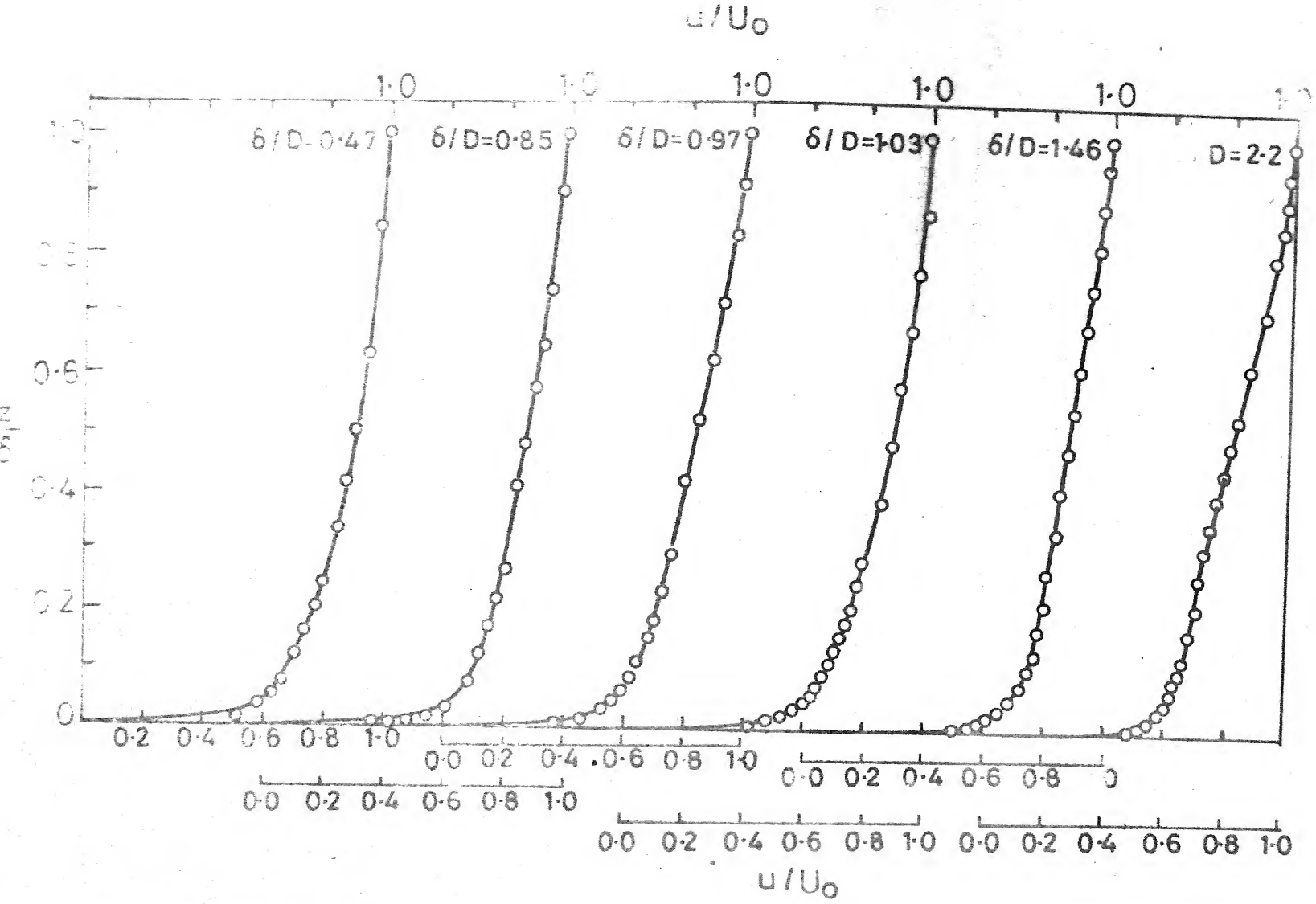

FIG.4.16 VELOCITY DISTRIBUTIONS ALONG THE CENTRE LINE AT X/D=5·0

Table 4.2 gives the summary of analysis of results of the investigation carried out in the wind tunnel.

4.6 Discussions:

Discussion is focused on the vortices developed in the separating region in plate and on the cylinder. It is attempted to relate the strength of vortices to the pressure distribution on the plate. The importance of the parameter $\delta/D.\ U_o/V_*$, in the scour studies has been discussed.

4.6.1 Strength of Vortices in Separating Region:

Pressure distribution of potential flow around circular cylinder will be a continuous rising curve from $C_p = 0.0$ at $\frac{r}{R} = \infty$ to $C_p = 1$ at $r/R = 1$, as can be seen from Eqn. 1.2. However, the pressure distribution on the plate at $\theta = 0$, from Fig. 4.7 is of a general rising curve but with a number of depressions or valleys along with it. Each depression is due to the presence of vortex in the separating region. Assuming vorticies are of forced types, having crest with edge of the vortex and through with the centre of the vortex, strength of each vortex must be proportional to the pressure difference between the crest and trough of a depression or a valley. An attempt to relate the strength of vortex with pressure difference is carried out below.

Pressure gradient in a forced vortex may be written as

$$\frac{1}{\rho}\frac{dP}{dr_*} = \frac{V_\theta^2}{r_*} = \omega^2 r_* \qquad (4.5)$$

where V_θ = tangential velocity of a forced vortex at radius, r_* and w is the angular velocity. In a forced vortex, angular velocity can be considered constant. Hence, Eqn. 4.5 can be integrated with limits $r_* = 0$, $P = P_c$ and $r_* = r_{*E}$ = edge of the vortex, $P = P_E$, one gets

$$\frac{P_E - P_C}{\rho} = \frac{\omega^2 r_{*E}^2}{2} \qquad (4.6)$$

Introducing Γ_f as strength of a forced vortex as

$$\Gamma_f = 2\pi r_{*E}. \quad (r_{*E}\omega) \qquad (4.7)$$

and nondimensionalising with $\pi D U_o$. Eqn. 4.7 simplifies to

$$\frac{\Gamma_f}{\pi D U_o} = \sqrt{\frac{P_E - P_C}{\frac{\rho U_o^2}{2}}} \left(\frac{2r_{*E}}{D}\right) = \left(\frac{2r_{*E}}{D}\right)\left(C_{PE-C}\right)^{1/2} \qquad (4.8)$$

where

$$C_{PE-C} = \frac{P_E - P_O}{1/2\rho U_o^2} - \frac{P_C - P_O}{1/2\rho U_o^2} = \text{difference in}$$

pressure co-efficient between edge and centre of the vortex. Pressure co-efficient difference C_{PE-C} refers only to the centre and edge of the vortex, which is above the plate in separating region. The presence of a vortex near the plate can also cause similar pressure depressions as

predicted by Eqn. 4.6. Representing C' and E' as the corresponding points to C and E of the vortex, distance CC' = r_{*E} and CE' = $\sqrt{2}\, r_{*E}$. Substituting $r_* = r_{*E}$ for $P = P'_C$ and $r_* = \sqrt{2}\, r_{*E}$ for $P = P'_E$, pressure difference $\frac{P'_E - P'_C}{\rho}$ can be shown equal to $\frac{P_E - P_C}{\rho}$. Valley in distribution measured on the plate is considered to represent the pressure difference between the centre and edge of the vortex. From Fig. 4.7, valley A a . B is considered as Vortex V_1, Valley B c C as vortex V_2 and Valley C c D as vortex V_3. The mean difference in pressure coefficients between the crests and troughs is denoted by C_{PE-C} and non-dimensional diameter of the vortex $2r_{*E}/D$, are measured from Fig. 4.7 and listed in the table below. Strength of vortex $\frac{\Gamma_f}{\pi D U_o}$ is computed from Eqn. 4.8 and velocity $V_{\theta E}$ at the edge of the vortex from Eqn. 4.5 as

$$\frac{V_{\theta E}}{U_o} = \left(\frac{\Gamma_f}{\pi D U_o}\right)\left(\frac{D}{2r_{*E}}\right) \qquad (4.9)$$

and are listed in the Table 4.0 shown below.

TABLE 4.0 : DETAILS OF VORTEX STRENGTH COMPUTATIONS

	Vortex V_1 (A a B)	Vortex V_2 (B b C)	Vortex V_3 (C c D)
	$\frac{\delta}{D} = 0.47$, $\frac{\delta U_o}{DV_*} = 12.17$		
C_{PE-C}	0.2	0.07	0.04
$\frac{2r_{*E}}{D}$	0.5	0.2	0.2
$\frac{\Gamma_f}{\pi DU_o}$	0.234	0.053	0.04
$\frac{V_{\theta E}}{U_o}$	0.407	0.40	0.2
	$\frac{\delta}{D} = 0.82$, $\frac{\delta U_o}{DV_*} = 19.50$		
C_{PE-C}	0.165	0.16	0.05
$\frac{2r_{*E}}{D}$	0.3	0.5	0.2
$\frac{\Gamma_f}{\pi DU_o}$	0.122	0.20	0.045
$\frac{V_{\theta E}}{U_o}$	0.407	0.40	0.223
	$\frac{\delta}{D} = 1.46$, $\frac{\delta U_o}{DV_*} = 46.02$		
C_{PE-C}	0.09	0.105	0.04
$\frac{2r_{*E}}{D}$	0.5	0.3	0.2
$\frac{\Gamma_f}{\pi DU_o}$	0.15	0.097	0.04
$\frac{V_{\theta E}}{U_o}$	0.30	0.32	0.2

contd....

Table 4.0 contd...

	Vortex V_1 (A a B)	Vortex V_2 (B b C)	Vortex V_3 (C c D)
	$\frac{\delta}{D} = 2.2$, $\frac{\delta U_o}{DV_*} = 83.26$		
C_{PE-C}	0.07	0.075	0.01
$\frac{2r_{*E}}{D}$	0.2	0.5	0.2
$\frac{\Gamma_f}{\pi D U_o}$	0.053	0.137	0.02
$\frac{V_{\theta E}}{U_o}$	0.266	0.274	0.1

From the above table, it may be observed strength of vortex V_1 and vortex V_2 will be of significant in magnitude in comparasion to vortex V_3. The velocity V_{0E} at the edge of vortex is found to be considerable (order of 0.4 U_o) for small values of δ/D and for larger values of δ/D., V_θ is order of 0.26 U_o.

4.6.2 Vortices on the Surface of Cylinder:

The pressure recovers gradually within the boundary layer thickness and then become more or less uniform outside the boundary layer as shown in the plot of pressure coefficient against z/δ at $\theta=0^o$ in Fig. 4.11. Also, there is no visible troughs and crests in the pressure distribution on the cylinder near the plate at $\theta=0^o$. It follows that at $\theta = 0^o$, there is possibility of absence of vortices on the cylinder. From the plots of pressure contours in the Fig.4.9 one or two regions of lowest pressure are found near the junction around 70-80°. These zones of the lowest pressures coincide with

the observed vortices in the paint impressions. This occurrence of vortices on both sides of the cylinder is due to corner vortex.

Another region of lowest pressure is also found at z/D = 3.6 to 4.0 around 80°. The pressure contours are lifted up towards this region. This indicates that vortices in the downstream side may be sucked up and shed in the wake at this height. This was also observed by Testsushi Okamoto and Miki Yagita (9).

4.6.3 Vorticity Parameter $\frac{\delta}{D}\frac{U_o}{V_*}$:

The strength of longitudinal vortex present in the boundary layer upstream of the cylinder is related to the vorticity parameter $\frac{\delta}{D}\frac{U_o}{V_*}$. Since this longitudinal vortex wraps around the cylinder in the corner, these vortices will be the cause for the possible scour occurrence on the erodible beds. For the fully developed uniform flow in open channels, 'δ' can be replaced by the depth of flow 'h' , V_* by $\sqrt{ghS}$ where S is energy slope. From this substitution, the parameter $\frac{\delta}{D}\frac{U_o}{V_*}$ simplifies as $\frac{h}{D}\frac{F_r}{\sqrt{S}}$ where F_r is Froude number of flow defined as $F_r = \frac{U_{avg}}{\sqrt{gh}}$. The energy slope (S) can be written from the the manning's equation,

$$\sqrt{S} = F_r \cdot \sqrt{g}\,\frac{n}{h^{1/6}} \qquad (4.12)$$

where n is 'mannings roughness coefficient'. Substituting for S in vorticity parameter, it simplifies as ,

$$\frac{\delta}{D} \cdot \frac{U_o}{V_*} = \frac{h}{D} \frac{F_r}{\sqrt{S}} = \frac{h}{D} \cdot \frac{h^{1/6}}{n} \cdot \frac{1}{\sqrt{g}} \qquad (4.13)$$

The mannings roughness coefficient (n) can be related to the median size of sediment on coarse sediment bed, as

$$n \propto d_{50}^{1/6} \qquad (4.14)$$

where d_{50} is the median size of sediment.

Rewriting the vorticity parameter in terms of 'd_{50}' ,

$$\frac{\delta}{D} \cdot \frac{U_o}{V_*} = K_* \frac{h}{D} \left(\frac{h}{d_{50}}\right)^{1/6} \qquad (4.15)$$

where K_* is a constant.

The equilibrium depth of scour in clear water shown by Laursen (4) is to be function of depth of flow and dimension of the pier and independent of Froude number. The present vortex parameter also substaintiates towards this understanding.

(C) Separation and Vortices Characteristics:

The distance of separation line on the plate from the centre of cylinder for $\theta = 0^{o}$ varies from 1.2 to 1.6 in the range of Reynolds numbers $R_{eD}=10^{2}$ to 10^{3} in water flume. Okamoto (10) investigation showed that a_{o}/D is around 1.6. Belik (10) related the distance of separation line from the centre of cylinder to the Reynolds numbers (R_{eD}). According to his proposed relations, a_{o}/D varies from 1.0 to 1.2 in the range of Reynolds number $R_{eD}=10^{4}$ to 10^{5}. Belik's relation underpredicts as per the present observations.

The average value of separation angle ($\bar{\theta}_{s}$) varies from 75^{o} to 90^{o} depending upon the flow conditions ($R_{eD}\approx 10^{3}$) in water flume. This can be compared with the location of laminar separation point ($R_{eD} = 10^{3}-10^{5}$) in a two dimensional cylinder held in a free stream which is at $\theta_{s} = 80^{o}-85^{o}$ (2).

Belik (1) obtained one valley in the pressure distribution on the plate for $\theta = 0^{o}$ at $r/R\approx 1.43$. Thus, he related this pressure distribution to the position of the vortex core at $r/R\approx 1.43$. Sarohia and Young (18) investigated two major vortices of reverse flow type and two small vortices of opposite sign to the main ones, one between the main ones and other deep in the junction. J.J. Cornish (3) reports the presence of two major vortices as can be seen in Fig. 1.1a and 1.1b. In the present investigation of pressure distribution on the plate at $\theta = 0^{o}$, three major vortices are postulated.

TABLE 4.1 : SUMMARY OF RESULTS OF FLOW VISUALISATION

Diameter of cylinder = 25 mm

Flow conditions	$F_r = \frac{U_{ave}}{\sqrt{gh}}$	0.143	0.200	0.316	0.322	0.473	1.31	1.467
	$R_{eD} = \frac{U_{ave} D}{\nu} \times 10^3$	0.300	0.500	0.610	0.520	0.950	1.48	1.45
	h/D	6.72	5.600	5.600	3.920	6.400	1.78	1.52
	Submerged conditions	Fully	Fully	Fully	Partia-lly	Fully	Par-tially	Partia lly
Results of Flow Pattern	$\frac{a_o}{D}$	1.640	1.480	1.220	1.460	1.380	1.640	1.46
	$\frac{a_{90}}{D}$	1.520	1.320	1.060	1.150	1.240	1.360	1.380
	$\bar{s}$ (mm)	9.700	4.600	8.500	3.750	8.300	3.700	4.700
	$\bar{s}/D$	0.388	0.184	0.340	0.150	0.332	0.148	0.188
	σ_s (mm)	0.175	0.052	0.157	0.056	0.113	0.079	0.089
	σ_s/D	0.070	0.021	0.063	0.022	0.045	0.032	0.036

a_o : Distance of separation line on the plate at $\theta = 0^o$ from the centre of cylinder

a_{90} : Distance of separation line on the plate at $\theta = 90^o$ from the centre of cylinder

$\bar{s}$: Average spacing of streaklines formed on the plate at upstream of cylinder

σ_s : Standard deviation of above streaklines.

TABLE 4.2 : SUMMARY OF ANALYSIS OF WIND TUNNEL DATA

U_o (m/s)	18.146	6.533	7.544	8.788	18.914	19.33
V_* (m/s)	0.701	0.259	0.310	0.326	0.600	0.511
$(\frac{\delta}{D})_{X/D=5.0}$	0.470	0.850	0.970	1.030	1.460	2.200
$R_{eD} = \frac{U_o D}{\nu}$ x10^5	0.600	0.220	0.250	0.290	0.630	0.645
$R_{e\delta} = \frac{U_o \delta}{\nu}$ x10^5	0.284	0.185	0.244	0.300	0.920	1.420
$R^*_{e\delta} = \frac{V_* \delta}{\nu}$ x10^3	1.100	0.730	1.000	1.100	2.900	3.700
$\frac{\delta}{D}\frac{U_o}{V_*}$	12.170	21.440	23.600	27.800	46.020	83.260
$(2\ell^*_y)_{ave} = \frac{\delta}{V_*}\frac{\partial u}{\partial z}$	44.000	93.100	89.100	107.600	158.700	306.900
$\bar{C}_D$	0.890	0.724	0.813	0.846	0.746	0.698

TABLE 4.3 : PRESSURE CHARACTERISTICS ON THE PLATE AT $\theta = 0^{\circ}$

$\frac{\delta}{D}$	$\frac{U_o}{V_*}$	$\bar{C}_p$	C_{pmax}	ΔC_{p1}	ΔC_{p2}	ΔC_{p3}	ΔC_{p4}
12.17		0.187	0.609	0.162	0.244	0.082	0.325
19.50		0.191	0.500	0.143	0.250	0.178	0.179
46.02		0.153	0.411	0.112	0.112	0.150	0.150
83.26		0.166	0.357	0.107	0.036	0.143	0.071

CHAPTER V

OBSERVATIONS, CONCLUSIONS AND RECOMMENDATIONS

From the analysis of flow pattern obtained by visualisation in water flume and the analysis of boundary layer flow conducted in the wind tunnel, the following observations and conclusions are drawn from the present investigation.

5.1 Observations:

A. Visualisation of Flow Pattern in Water Flume:

(a) The distance of separation line on the plate at $\theta = 0$, is around $\frac{X}{D} \approx 1.5$ from the centre of cylinder.

(b) The occurrence of number of lines in the separation region on the plate shows a number of vortices.

(c) The average separation angle ($\bar{\theta}_s$) on the surface of cylinder varies from 75^o to 90^o depending upon the flow conditions. In general, $\bar{\theta}_s$ increases with increasing Froude number and Reynolds number (R_{eD}).

(d) Flow patterns are greatly affected by the submerged conditions.

B. Pressure Distributions:

(a) From the pressure contours on the plate, the intense pressure distribution is observed inside the separation region.

(b) The pressure distribution on the plate at $\theta = 0^{o}$ shows a number of crests and troughs.

(c) The minimum pressure coefficient on the surface of cylinder occurs between $\theta = 70^{o}$ and $\theta = 90^{o}$. The separation of flow on the surface of cylinder is also believed to occur at this range of angles.

(d) The gradual recovery of pressure on the surface of cylinder at $\theta = 0$ takes place inside the boundary layer thickness.

(e) From the pressure contours on the surface of cylinder, occurrence of vortices behind the cylinder is observed. These vortices are sucked up and supposed to be shed in the wake at the height of $z/D = 3.6$ to 4.0, where the concentration of vortices is observed by the low pressures.

5.2 Conclusions:

(1) The **lateral** vortices in the upstream boundary layer flow between $0.01 \leq z/\delta \leq 0.2$ are found to follow logarithmic velocity distribution. The average of the upstream **lateral** vorticity is **function of** the parameter $\frac{\delta}{D} \frac{U_o}{V_*}$.

(2) In the present investigation, three-major vortices are found to be present from the pressure distribution in the separation region on the plate at the front of

cylinder. The strength of these vortices (horse-shoe vortices) occuring inside the separation region on the plate can be related to the pressure distribution on the plate. The strength of vortices is proportional to the square root of difference in pressure coefficients between centre and edge of vortices. Since pressure distribution on the plate is function of upstream boundary layer flow, therefore, the strength of vortices occuring in the separation region can be related to the upstream average **lateral** vorticity or upstream vorticity parameter $\frac{\delta}{D}\ \frac{U_o}{V_*}$.

(3) The gradual recovery of pressure coefficient with z/δ, on the surface of cylinder at $\theta = 0$ follows one distribution for all boundary layers.

(4) Drag coefficient increases gradually along the height of cylinder from the plate till the edge of boundary layer and then remains fairly constant outside the boundary layer. The smoothing of sharpness of crest of the maximum drag coefficient takes place with increasing boundary layer thickness. The average form drag coefficient decreases with the parameter $\frac{\delta}{D}\ \frac{U_o}{V_*}$.

(5) The vorticity parameter $\frac{\delta}{D}\ \frac{U_o}{V_*}$ which is equivalent to $\frac{h}{D}\ \frac{F_r}{\sqrt{S}}$ in uniform open channel flows, can be well related to the equilibrium scour depth occuring due to horse-shoe vortices.

5.3 Recommendations for Future Studies:

For further studies, it is suggested to investigate the flow characteristics past the cylinder making model of scour hole around the cylinder. It will be very interesting to investigate the distributions of pressures and vortices inside the scour hole. It will also be suggested to conduct same investigation on the mobile bed, so that mechanism of scour can be well related to the horse-shoe vortices.

REFERENCES

1. Belik, L. (1973) : 'Secondary Flow About Circular Cylinders Mounted Normal to a Flat Plate', Aeronautical Quarterly Vol.24, Feb. 1973, Part 1, pp. 47-54.
2. Chang, Paul K. (1970): 'Separation of Flow', Vol. 3, Pergamon Press.
3. J.J. Cornish III: 'Vortex Flows', Engineering and Advanced Programs, Lockheed-Georgia Company, U.S.A.
4. Laursen, E.M. (1960): 'Scour at Bridge Crossings', Journal of Hyd. Div. A.S.C.E., Vol.86, No. HY2, Proc. Paper 2369 Feb., pp. 39-54.
5. Laursen, E.M. (1962): 'Scour at Bridge Crossings', Transactions, A.S.C.E., Vol. 127, Part 1, 1962, pp. 166-180.
6. Laursen, E.M. and Toch, A. (1956): Bulletin No. 4, IOWA Highway Research Board, May 1956.
7. Masch, F.D. and Morre, W.L. (1960): 'Drag Forces in Velocity Gradient Flow', J.of Hyd. Div. Proc. A.S.C.E., Vol. 86, No. HY7, pp. 2546.
8. Masaru, Kiya and Mikio Arie (1975): 'Viscous Shear Flow Past Small Bluff Bodies Attached to a Plane Wall', J. of Fluid Mech., Vol.69, Part 4, 1975, pp. 803-823.
9. Okamoto, Tetsushi and Miki Yagita (1973): 'The Experimental Investigation on the Flow Past a Circular Cylinder of Finite Length Placed Normal to the Plane Surface in a Uniform Stream', Bulletin of J.S.M.E., Vol.16, No.95, May 1973, pp. 805-814.

10. Okamoto, S. (1981): 'Turbulent Shear Flow Behind Hemisphere Cylinder Placed on Ground Plane', Turbulent Shear Flows 3 (The Third International Symposium on Turbulent Shear Flows, The University of California Davis, Sept.9-11, 1981).

11. Pankhurst, R.C. and Holder,D.W. (1948): 'Wind-Tunnel Technique', Sir Isaac Pitman and Sons Ltd. London, Chapter 8.

12. Pillai, A. Sankaranarayana (1981): 'Flow Past Circular Cylinders at Different Blockages', M.E. Thesis, Water Res. Development Training Centre, University of Roorkee, Roorkee.

13. Posey, C.J. (1949): 'Why Bridge Fails in Floods', Civil Engg.,' Vol. 19, Feb., pp. 42-90.

14. Ramamurthy, A.S. and Ng, C.P. (1973): 'Effect of Blockage on Steady Force Coefficients', Journal of Engg. Mech. Div., Proc. A.S.C.E., Vol.99, Em4, 1973, pp. 755.

15. Rana, O.P.S. (1980): 'Flow Past Circular Cylinders in Open Channels', M.E. Thesis, Hydraulic Engg. Section, Department of Civil Engineering, University of Roorkee Roorkee.

16. Ranga Raju, K.G. and Vijay Singh (1975): 'Blockage Effects on Drag of Sharp-edged Bodies', Journal of Ind. Aerodynamics, Vol.1, 1975-76, pp. 301.

17. Roper, A.T., Schneider, V.R. and Shen, H.W. (1967): 'Analytical Approach to Local Scour', Pre-Congress Vol.3, Proc. Paper No. C18, June, for XII Congress of I.A.H.R., Fort Collins, Colorado.

18. Sarohia, S. and A.D. Young (1982): 'Wind-Tunnel Investigations of Some Three-Dimensional Separated Turbulent Boundary Layers', I.U.T.A.M. Symposium, Berlin, Germany, March 29-April 1, 1982.

19. Schlichting, H.; 'Boundary Layer Theory', Fourth Editions, McGraw Hill Book Company.

20. Sharpe, G.J. (1969) : 'Fluid Flow Analysis', Heinemann Educational Books Ltd., London.